Journal of Atmospheric and Solar-Terrestrial Physics 168 (2018) 80–99

Contents lists available at ScienceDirect

Journal of Atmospheric and Solar-Terrestrial Physics

journal homepage: www.elsevier.com/locate/jastp

Modeling of tropospheric NO_2 column over different climatic zones and land use/land cover types in South Asia

Zia ul-Haq *, Asim Daud Rana, Salman Tariq, Khalid Mahmood, Muhammad Ali, Iqra Bashir

Remote Sensing and GIS Group, Department of Space Science, University of the Punjab, New Campus, Lahore 54590, Pakistan

ARTICLE INFO

Keywords:
NO_2
Regression analysis
Air pollution
Climate change
OMI

ABSTRACT

We have applied regression analyses for the modeling of tropospheric NO_2 (tropo-NO_2) as the function of anthropogenic nitrogen oxides (NO_x) emissions, aerosol optical depth (AOD), and some important meteorological parameters such as temperature (Temp), precipitation (Preci), relative humidity (RH), wind speed (WS), cloud fraction (CLF) and outgoing long-wave radiation (OLR) over different climatic zones and land use/land cover types in South Asia during October 2004–December 2015. Simple linear regression shows that, over South Asia, tropo-NO_2 variability is significantly linked to AOD, WS, NO_x, Preci and CLF. Also zone-5, consisting of tropical monsoon areas of eastern India and Myanmar, is the only study zone over which all the selected parameters show their influence on tropo-NO_2 at statistical significance levels. In stepwise multiple linear modeling, tropo-NO_2 column over landmass of South Asia, is significantly predicted by the combination of RH (standardized regression coefficient, $\beta = -49$), AOD ($\beta = 0.42$) and NO_x ($\beta = 0.25$). The leading predictors of tropo-NO_2 columns over zones 1–5 are OLR, AOD, Temp, OLR, and RH respectively. Overall, as revealed by the higher correlation coefficients (r), the multiple regressions provide reasonable models for tropo-NO_2 over South Asia ($r = 0.82$), zone-4 ($r = 0.90$) and zone-5 ($r = 0.93$). The lowest r (of 0.66) has been found for hot semi-arid region in northwestern Indus-Ganges Basin (zone-2). The highest value of β for urban area AOD (of 0.42) is observed for megacity Lahore, located in warm semi-arid zone-2 with large scale crop-residue burning, indicating strong influence of aerosols on the modeled tropo-NO_2 column. A statistical significant correlation ($r = 0.22$) at the 0.05 level is found between tropo-NO_2 and AOD over Lahore. Also NO_x emissions appear as the highest contributor ($\beta = 0.59$) for modeled tropo-NO_2 column over megacity Dhaka.

1. Introduction

The atmospheric nitrogen oxides ($NO_x = NO + NO_2$), especially NO_2, adversely impacts human health and the natural environment (Case et al., 1979; Barck et al., 2005). NO_x and hydrocarbons are correlated with surface level ozone (Varotsos et al., 1992). The tropospheric NO_2 (tropo-NO_2) pollution is greatly influenced by spatial patterns of socio-economics as well as by the changes in meteorological conditions, and topographic attributes (elevation, land use and land cover) of the area (Parra et al., 2009).

NO_2 largely comes from industrial and vehicle combustion processes, biomass and crop-waste burning, soil emissions, and sky lightning (Richter and Burrows, 2002; Cheng et al., 2012). NO_2 is mainly removed from the atmosphere by its reaction with OH (Kanaya et al., 2007). The changes in meteorological parameters (e.g., air temperature, relative humidity, wind speed, precipitation, solar radiation, and cloud fraction), atmospheric chemistry and surface emissions largely determine seasonally dependent NO_2 concentrations (Ghude et al., 2009; Sheel et al., 2010; ul-Haq et al., 2014).

Several researchers have explained and modeled trace gases variations by employing polynomial, multiplicative and multiple linear regression models (e.g., Varotsos et al., 1992, 2014a,b; Clapp and Jenkin, 2001; Kondratyev and Varotsos, 2001; Ferm et al., 2005; Sheel et al., 2010; Han et al., 2011). The adequate performance of the regression models help to assess the air quality and formulate localized environmental protection policies (Varotsos et al., 1992).

Multiple linear regression (MLR) has become a well-known and effective technique for predicting relationships and modeling the environmental systems (Demuzere and van Lipzig, 2010). This study suggests the relationship of tropo-NO_2 with anthropogenic nitrogen oxides (NO_x) emissions, some important meteorological parameters such as air temperature (Temp), relative humidity (RH), wind speed (WS), precipitation

* Corresponding author.
E-mail address: zia.spsc@yahoo.com (Z. ul-Haq).

https://doi.org/10.1016/j.jastp.2018.01.022
Received 25 January 2017; Received in revised form 13 January 2018; Accepted 15 January 2018
Available online 22 January 2018
1364-6826/

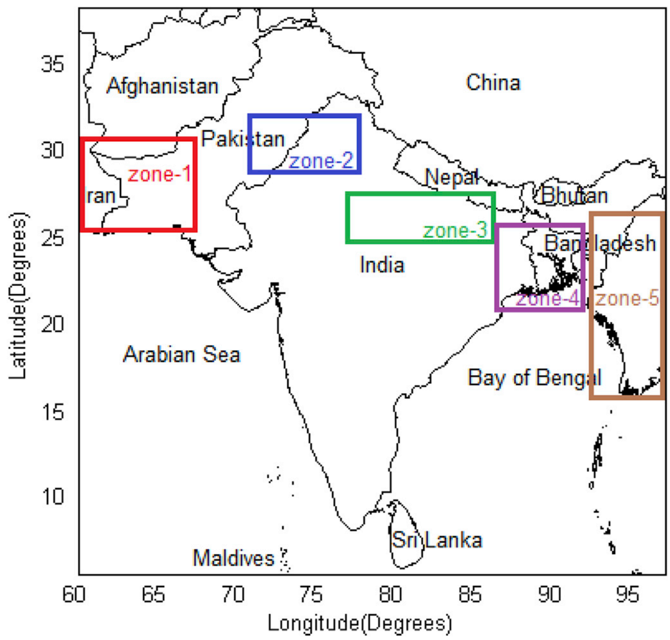

Fig. 1. Geographical map of South Asia and five study zones (1–5).

Table 1
The spatial bounding of the zones along with important anthropogenic sources of NO_2. Köppen-Geiger climate classification based on native vegetation, temperature, precipitation and their seasonality (Kottek et al., 2006) is also included.

Zones	Spatial bounding	Climate classification and population density	Notable sources of NO_2
Zone-1	25.5–31.5°N,60.5–69.5°E	Warm desert (BWh), very low density	Gawadar and Chahbhar Ports activities, fossil fuel burning
Zone-2	28.5–32.5°N,72.5–76.5°E	Hot semi arid (BSh), High density	Crop residue burning (post and pre monsoon), megacities (Lahore, Delhi, Faisalabad), industries, winter time home heating, brick kilns, power plants
Zone-3	24.5–26.5°N,76.5–85.5°E	Subtropical humid summer, dry winter (Cwa), High density	Crop residue burning (post and pre monsoon), industries, winter time home heating, brick kilns, power plants
Zone-4	20.5–25.5°N,85.5–92.5°E	Tropical savanna, wet & dry (Aw), very High density	Crop residue burning (pre-monsoon), mining activities, power plants, industries, brick kilns, urban
Zone-5	15.5–25.5°N,92.5–97.5°E	Tropical monsoon (Am), low density	Crop residue burning (pre monsoon), megacity Dhaka, power plants

(Preci), outgoing long wave radiation (OLR), cloud fraction (CLF) and aerosol optical depth (AOD) by using bi-variate and multivariate linear regression methods over different climatic zones and land use/land cover (LULC) types in landmass of South Asia.

2. Material and methods

2.1. Location and description of the study area

South Asia is home to one-fourth of the global population with population over 1.667 billion (Joshi, 2015; Li et al., 2015). Eight countries form South Asia namely Afghanistan, Bangladesh, Bhutan, India, Maldives, Pakistan, Nepal and Sri Lanka covering total surface area of 5, 134,613 km^2 (Fig. 1). Its climatic conditions fluctuate from arctic temperatures in the northern Himalayan areas to a temperate climate in the foothills and northern Indus-Ganges Basin (IGB). The tropical conditions are observed in central Indian Deccan plateau. The meteorological conditions of South Asia are heavily affected by wet (summer) and dry (winter) monsoon systems causing alternating periods of wet and dry weather (UNEP, 2008; Joshi, 2015). To perform in-depth analysis, we have formed five study zones (1–5) based on different climatic conditions and LULC types in South Asia (Fig. 1). The details of these zones are given in Table 1 along with important sources of anthropogenic NO_2.

Seasonal mean maps have been generated for some important meteorological parameters such as relative humidity, surface air temperature, wind speed and precipitation rate in South Asia for a period of December 1999 to November 2012 (Fig. 2). These maps are based on the data generated using NCEP-NCAR Reanalysis facility provided at NOAA Earth System Research Laboratory (NOAA-ESRL), Physical Sciences Division (www.esrl.noaa.gov/psd/).

2.2. Data

Ozone Monitoring Instrument (OMI, Levelt et al., 2006) on board Aura satellite is providing global coverage of tropo-NO_2 measurements since 2004. OMI tropo-NO_2 columns generally show a good agreement with ground-based measurements and are underestimated by 15–30% (Celarier et al., 2008). Differential Optical Absorption Spectroscopy (DOAS) algorithm uses radiance from 405 to 465 nm to retrieve tropo-NO_2. Daily retrievals of tropo-NO_2 (OMNO2d v003, level-3, and version-3) gridded at $0.25° \times 0.25°$ during a time period from October 2004 to December 2015 have been used in the present study. Tropo-NO_2 data are obtained from Giovanni (2016). Details of DOAS analysis and data quality control are provided in OMI data user's guide (OMI, 2012) and in Bucsela et al. (2006, 2008, 2013).

Gridded data of NO_x anthropogenic emissions have been obtained from Monitoring Atmospheric Composition and Climate (MACC) and megaCITY-Zoom for the Environment, CityZEN project (MACCity, Granier et al., 2011; ul-Haq et al., 2017). MACCity inventory is based on anthropogenic NO_x emissions from energy, transportation, industrial, residential and agricultural sectors. MODerate resolution Imaging Spectro-radiometer (MODIS) sensor aboard Aqua satellite was launched in 1999 (Salomonson et al., 1989). It uses 36 spectral bands (0.4–14.4 μm) with high radiometric resolution at 12 bits to monitor global radiation budget, aerosol burden and cloud cover on daily basis (Kaufman et al., 1997). Different algorithms are used for aerosols retrievals over land and oceans employing MODIS radiances (Kaufman et al., 1997; Tanre et al., 1997). In this study, we have adopted MODIS/Aqua deep blue Aerosol Optical Depth (AOD) monthly product (MYD08_M3, level-3, collection-6) with $1° \times 1°$ spatial resolution. The collection-6 of AOD is the latest and significantly improved product based on long-term calibration, improved cloud masking and atmospheric profile algorithms.

Some important meteorological parameters have been obtained from Atmospheric Infrared Sounder (AIRS, Pagano et al., 2003) and The Advanced Microwave Sounding Unit-A (AMSU-A, Aumann et al., 2003) on board NASA's Aqua satellite. The simultaneous use of AIRS and AMSU-A provides both new and improved measurements (Aumann et al., 2003; Susskind et al., 2003). These AIRS/AMSU-A derived meteorological parameters are cloud fraction, atmospheric temperature at 925 hPa, relative humidity at 925 hPa, and top of the atmosphere (TOA)

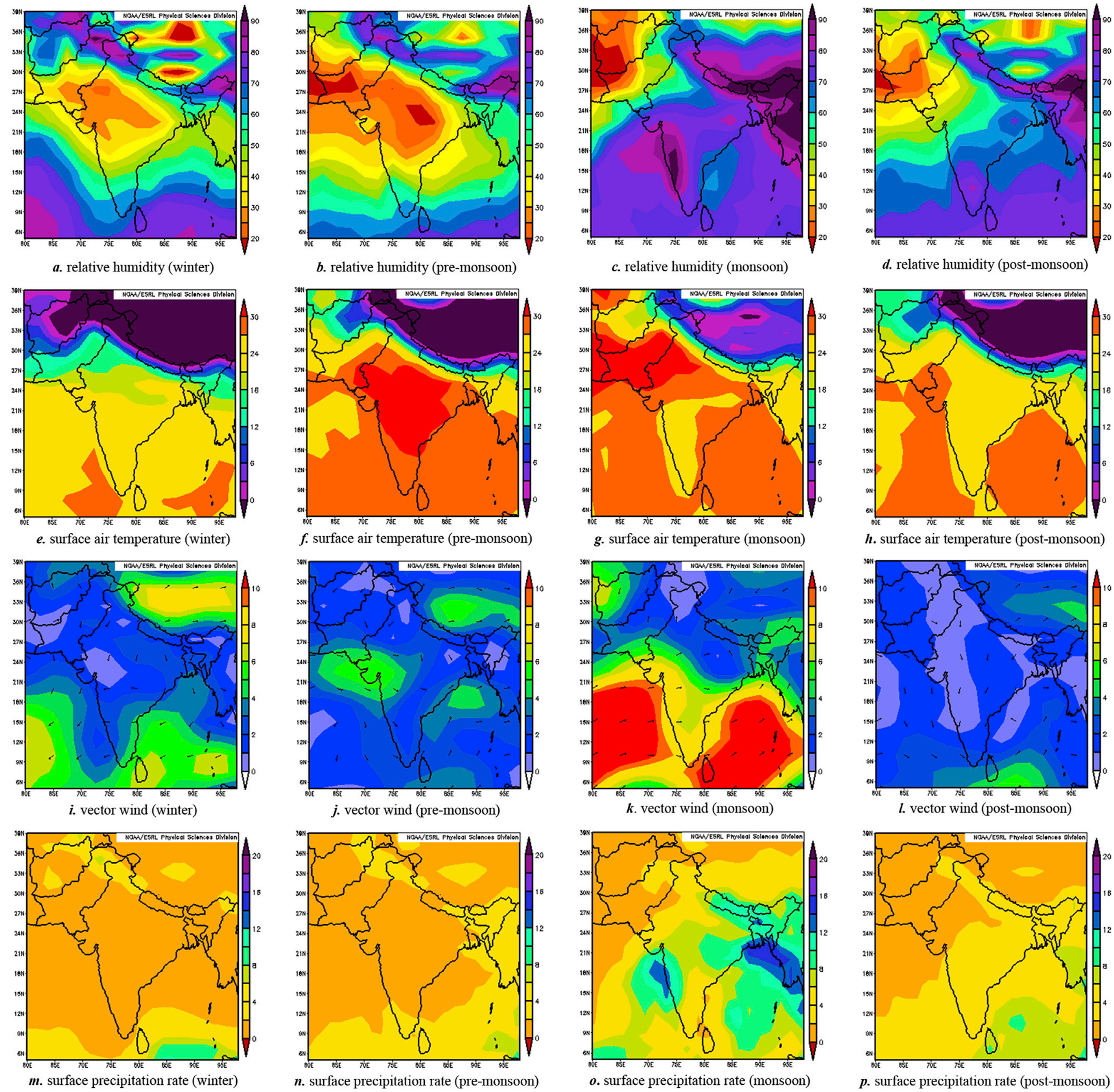

Fig. 2. Seasonal maps of relative humidity (%, at 925 hPa), air temperature (°C, at surface), vector wind (m s^{-1}, at 925 hPa), and precipitation rate (mm/day, at surface) of the study area for a period from December 1999 to November 2012. These maps have been generated using NCEP-NCAR Reanalysis facilitated at NOAA-ESRL-PSD.

outgoing long-wave radiation for clear sky.

In addition to the data described above, surface level precipitation rate and near surface wind speed data have been obtained from Tropical Rainfall Measuring Mission (TRMM, Liu et al., 2012) and Global Land Data Assimilation System (GLDAS, Fang et al., 2009), respectively. The details of all the datasets used in this study are given in Table 2.

2.3. Methodology

Tropo-NO_2 is anti-correlated with temperature, relative humidity, precipitation and wind speed (Arya, 1999; Jones et al., 2010; Ramachandran et al., 2013). Also, the direct coupling of tropo-NO_2 with outgoing long-wave radiation (OLR), linked to cloud cover and convective activities, and indirect through the absorption of OLR by tropospheric ozone are reported by several authors (e.g. Worden et al., 2011; David and Nair, 2013; Varotsos et al., 2014a,b). Aerosols also participate in the modulation of NO_2 levels. The formation of Secondary Organic Aerosols (SOA) may be seen as a notable sink of NO_2 (Kroll and Seinfeld, 2008; Hallquist et al., 2009). Aerosols have commonality of some important emission sources with NO_2 such as fossil fuel combustion, biomass and crop waste burning, industries and organic compounds. Also aerosols alter the radiation budget and contribute to the formation of clouds thus influencing the photochemistry of NO_2 (Seinfeld and Pandis, 1998).

Table 2
Details of datasets obtained from satellite sensors and model used in this study.

Product name (identifier)	Sensor/ Model	Retrieval time (day/night)	Spatial resolution (degrees)	Product name/version/level	Units	Level description
NO_2 (OMNO2d v003)	OMI	daytime	$0.25° \times 0.25°$	version-3/level-3	($\times 10^{15}$ molecules cm^{-2}	Tropospheric
AOD (MYD08_M3)	MODIS	daytime	$1° \times 1°$	version-6/level-3	Unit less	Total column
Anthro-NO_x	MACCity	–	$0.5° \times 0.5°$	–	kg $m^{-2} s^{-1}$	Surface emissions
Cloud fraction (AIRX3STM)	AIRS/ AMSU-A	daytime	$1° \times 1°$	version-6/level-3	Unit less	Total column
Temperature (AIRX3STM)	AIRS/ AMSU-A	daytime	$1° \times 1°$	version-6/level-3	Kelvin	925 hPa
Relative humidity (AIRX3STM)	AIRS/ AMSU-A	daytime	$1° \times 1°$	version-6/level-3	%	925 hPa
Outgoing long-wave radiation (AIRX3STM)	AIRS/ AMSU-A	daytime	$1° \times 1°$	version-6/level-3	W m^{-2}	Top of the atmosphere
Precipitation rate (3B43)	TRMM	daytime	$0.25° \times 0.25°$	version-7/level-3	mm $month^{-1}$	Surface level
Wind speed (GLDAS_NOAH025_M)	GLDAS Model	–	$0.25° \times 0.25°$	GLDAS_NOAH025_M/version-2.1/level-3	m s^{-1}	Near surface level

Tropo-NO_2 modeling has been divided into two types: simple linear regression modeling and stepwise multiple linear regression modeling (e.g., Engel-Cox et al., 2004; Lin et al., 2012). Simple linear regression model is a simple empirical model used to find the association between tropo-NO_2, NO_x, AOD and meteorological factors separately. Simple linear regression technique is given in Eq. (1), where a_o is an intercept while b *is* the regular (unstandardized) regression coefficient (Dancey and Reidy, 2014), and w is the regressor. In regression analysis for only one regressor, the standardized regression coefficient (β) has the same value as the correlation coefficient (r) between the two variables (Aron et al., 2013).

$$\textit{Monthly tropo-}NO_2 = a_o + bw \tag{1}$$

To improve the results of the proposed models presented in the section 3.1.*a*, a stepwise multiple linear regression technique is used that includes AOD, NO_x, RH, Preci, Temp, WS, CLF and OLR. These models incorporate the stepwise regression procedure presented by Lin et al. (2012). Commonly, this procedure involves "enter" and "remove" processes. The first process of "enter" will add each variable into the regression equation only if it significantly increases the correlation of the model equation. AOD, NO_x, and selected meteorological variables are entered in descending order of their individual correlations with tropo-NO_2. A significance level of 0.01 has been set for selection criteria for variables for South Asia and the study zones. If the previously added variable loses its explanatory power below a certain range, after the new variable added in the model equation, then this variable is removed from the model equation. The stepwise procedures are based on an F-statistic, that is the square of the t-statistic, the criterion Probability-of-F-to-enter $\leq$ 0.05 is used to enter a regressor into the model, and the condition Probability-of-F-to-remove $\geq$ 0.10 is applied to remove a regressor from the model. Tropo-NO_2 is set to be a dependent variable. As NO_2 variability is generally modulated by meteorological parameters, NO_x and AOD (Veefkind et al., 2011; ul-Haq et al., 2017), these are selected as independent variables. Stepwise multiple linear regression is given in Eq. (2), where a_o is an intercept while b_1, b_2, b_3, b_4, b_5, b_6, b_7 and b_8 are the regular (unstandardized) regression coefficients. The regressors of these analysis are AOD, NO_x, RH, Preci, Temp, CLF, WS and OLR.

$$\text{Monthly tropo-}NO_2 = a_o + b_1\,\text{AOD} + b_2\,NO_x + b_3\,\text{RH} + b_4\,\text{Preci} + b_5\,\text{Temp} + b_6\,\text{CLF} + b_7\,\text{WS} + b_8\,\text{OLR} \tag{2}$$

This multiple regression examines the underplaying relationship of tropo-NO_2, NO_x, AOD and selected meteorological factors, provides better predictability than the simple linear models, and more importantly their relative impacts. It is seen that the inclusion of meteorological parameters has greatly increased the correlations of the equations and decreased the standard errors of the models for South Asia and all the study zones. The outputs of multiple regressions reveal some interesting and variety of results. A standardized regression coefficient (β, Dancey and Reidy, 2014), used to compare the relative effects of regressors measured on different scales, shows the predicted amount of change in standard deviation units of the criterion variable if the value of the predicted variable increases by one standard deviation (Aron et al., 2013).

The monthly means of tropo-NO_2 are obtained by averaging the daily observations during a given month. For the reliability of the results, spatial correlations between monthly mean tropo-NO_2 and other factors have been calculated for only those grid points which have at least 12 values of monthly mean data.

3. Results and discussion

The yearly mean column of OMI tropo-NO_2 over landmass of South Asia has significantly increased by 14.7% (*slope*: 0.014×10^{15} molecules cm^{-2} and correlation coefficient $r = 0.89$) with an average of $1.1 \pm 0.05 \times 10^{15}$ molecules cm^{-2} during 2005–2015 (Table 3). This increase is in confirmation with Ghude et al. (2008, 2009) and ul-Haq et al. (2015). The major causes of tropo-NO_2 growth over the study zones and South Asia, given in Table 1, are increasing anthropogenic activities associated with industrial, power, agricultural, traffic and urban sectors (Azad and Kitada, 1998; Ghose et al., 2004; Badarinath et al., 2006, 2009; Ghude et al., 2008, 2009; Gurjar et al., 2008; Renuka et al., 2014; Ali et al., 2014; ul-Haq et al., 2014, 2015; Tariq and Ali, 2015).

The tropo-NO_2 concentration is significantly modulated by local meteorological conditions, solar radiation dependent photolysis rate, local emissions, aerosols loading, hydroxyl radical concentration and water content in the troposphere. The meteorological conditions i.e. wind speed, precipitation, temperature, humidity and solar radiations affect NO_2 abundance via removal, transformation and transport processes (Arya, 1999). An enhancement of NO_2 photolysis is observed in hot and humid atmosphere (Ramachandran et al., 2013). Also strong winds dilute NO_2 column near emission sources through transport and enhanced vertical air mixing (Arya, 1999; Ramachandran et al., 2013; Jones et al., 2010). NO_2 and aerosols are related through the conversion of NO_2 into secondary organic aerosols (Kroll and Seinfeld, 2008; Hallquist et al., 2009), commonality of major emission sources (Veefkind et al., 2011) and modification of the Earth's radiation budget by aerosols that alter NO_2 photochemistry (Seinfeld and Pandis, 1998).

The highest tropo-NO_2 annual mean value of 2.5 ± 0.1 ($\times 10^{15}$ molecules cm^{-2}) with 17.4% growth rate has been noted over zone-2 consisting of northern Indus Basin (IB) and western Ganges Basin (GB) parts linked to high anthropogenic emissions. This zone has two megacities Lahore and Delhi, and large crop residue burning areas. The highest tropo-NO_2 growth rate of 22.1% is found for zone-4. This study zone consists of eastern mining region of India and heavily populated areas of

Table 3
Annual and seasonal means, and overall change (%) based on annual means of NO_2 ($\times 10^{15}$ molecules cm^{-2}), NO_x ($\times 10^{-11}$ kg m^{-2} s^{-1}), aerosol optical depth (AOD, unit less), temperature at 925 hPa (K), surface wind speed (WS, m s^{-1}), precipitation rate (Preci, mm $month^{-1}$), cloud fraction (CLF, unit less), outgoing long-wave radiation (OLR, W m^{-2}) and relative humidity (RH, %) for the five study zones and South Asia during October 2004–December 2015.

		Annual	Winter	Pre-monsoon	Monsoon	Post-monsoon	Overall Change (%) relative to 2005
NO_2	South Asia	1.1 ± 0.05	0.89 ± 0.06	0.97 ± 0.06	0.8 ± 0.08	0.79 ± 0.07	14.7
	Zone-1	0.9 ± 0.03	0.72 ± 0.03	0.77 ± 0.04	1.17 ± 0.09	0.82 ± 0.05	10.8
	Zone-2	2.5 ± 0.12	2.01 ± 0.07	2.60 ± 0.04	3.14 ± 0.06	2.48 ± 0.06	17.4
	Zone-3	2.03 ± 0.07	2.02 ± 0.04	2.05 ± 0.04	1.96 ± 0.03	1.97 ± 0.06	11.6
	Zone-4	1.9 ± 0.13	2.10 ± 0.07	2.13 ± 0.06	1.37 ± 0.04	1.65 ± 0.07	22.1
	Zone-5	1.06 ± 0.07	0.95 ± 0.07	1.73 ± 0.07	0.51 ± 0.04	0.60 ± 0.06	3.9
NO_x	South Asia	1.36 ± 0.13	1.44 ± 0.17	1.40 ± 0.17	1.47 ± 0.14	1.39 ± 0.15	44.0
	Zone-1	0.87 ± 0.01	0.86 ± 0.008	0.9 ± 0.008	1.0 ± 0.008	0.9 ± 0.008	31.4
	Zone-2	5.52 ± 0.82	5.92 ± 0.83	5.72 ± 0.84	6.20 ± 0.79	5.63 ± 0.83	55.0
	Zone-3	5.67 ± 0.84	6.17 ± 0.85	5.9 ± 0.84	6.16 ± 0.83	5.7 ± 0.86	82.5
	Zone-4	5.13 ± 0.69	5.77 ± 0.69	5.27 ± 0.73	5.4 ± 0.66	5.21 ± 0.7	55.0
	Zone-5	0.5 ± 0.004	0.53 ± 0.004	0.55 ± 0.004	0.5 ± 0.003	0.5 ± 0.004	27.5
AOD	South Asia	0.29 ± 0.01	0.266 ± 0.03	0.34 ± 0.03	0.303 ± 0.06	0.24 ± 0.02	10.1
	Zone-1	0.22 ± 0.02	0.17 ± 0.04	0.23 ± 0.01	0.34 ± 0.03	0.17 ± 0.04	3.6
	Zone-2	0.5 ± 0.03	0.41 ± 0.03	0.43 ± 0.02	0.69 ± 0.07	0.48 ± 0.02	−0.9
	Zone-3	0.46 ± 0.02	0.54 ± 0.03	0.39 ± 0.02	0.44 ± 0.04	0.45 ± 0.03	18.5
	Zone-4	0.45 ± 0.04	0.51 ± 0.02	0.45 ± 0.03	0.45 ± 0.03	0.38 ± 0.02	33.6
	Zone-5	0.28 ± 0.01	0.16 ± 0.06	0.41 ± 0.06	0.36 ± 0.02	0.20 ± 0.03	3.3
Temp	South Asia	295.9 ± 0.2	291.8 ± 0.4	297.8 ± 0.5	298.3 ± 0.3	295.7 ± 0.2	−0.1
	Zone-1	299.7 ± 0.3	289.2 ± 1.2	302 ± 1.4	307.9 ± 0.7	300 ± 1	−0.2
	Zone-2	295.9 ± 0.4	286.2 ± 1.2	299 ± 1.4	302.1 ± 0.9	296.4 ± 0.7	−0.3
	Zone-3	297.3 ± 0.5	290.3 ± 1.1	301.9 ± 1.2	300.3 ± 1	296.6 ± 0.6	−0.3
	Zone-4	295.4 ± 0.3	290.7 ± 0.7	298.1 ± 0.8	297.8 ± 0.4	295 ± 0.3	−0.1
	Zone-5	296 ± 0.2	293.2 ± 0.6	298.2 ± 0.6	296.9 ± 0.2	295.6 ± 0.2	0.1
WS	South Asia	3.6 ± 0.1	3.7 ± 1.9	3.8 ± 2	3.8 ± 2	3.1 ± 1.6	2.9
	Zone-1	3.7 ± 0.1	3.4 ± 1.8	3.9 ± 2	4.3 ± 2.2	3.2 ± 1.6	4.0
	Zone-2	2.7 ± 0.1	2.8 ± 1.4	3.2 ± 1.6	2.5 ± 1.3	2.4 ± 1.2	4.4
	Zone-3	2.1 ± 0.1	2.02 ± 1.04	2.47 ± 1.28	2.26 ± 1.17	1.64 ± 0.84	−3.3
	Zone-4	2.2 ± 0.1	2 ± 1.1	2.5 ± 1.3	2.3 ± 1.2	1.9 ± 1	−3.8
	Zone-5	1.9 ± 0.1	1.9 ± 1	2.06 ± 1.1	1.9 ± 1	1.5 ± 0.8	−0.8
Preci	South Asia	98.1 ± 6	38.4 ± 9.7	58.5 ± 13.5	185.9 ± 20.6	109.3 ± 15.3	−2.7
	Zone-1	15.8 ± 3.02	22.6 ± 18.8	15.5 ± 9.4	18.8 ± 16	6.8 ± 8	−18.5
	Zone-2	42.1 ± 8.1	19.9 ± 14.8	24.5 ± 19.5	91.3 ± 41.1	33.2 ± 19.7	34.8
	Zone-3	84.1 ± 16.6	14.6 ± 15.2	14 ± 10.7	243.1 ± 79.7	64.3 ± 35.9	2.2
	Zone-4	163.8 ± 17	12.3 ± 14.7	90.3 ±42.9	391.3 ± 94	162.3 ± 59.1	−9.7
	Zone-5	199.3 ± 16.4	7.7 ± 9.8	114.6 ± 37	478.9 ± 59.7	194.1 ± 45.5	−0.9
CLF	South Asia	0.34 ± 0.01	0.25 ± 0.02	0.28 ± 0.02	0.50 ± 0.03	0.34 ± 0.03	0.1
	Zone-1	0.17 ± 0.01	0.21 ± 0.07	0.19 ± 0.05	0.18 ± 0.04	0.10 ± 0.03	−5.7
	Zone-2	0.19 ± 0.02	0.20 ± 0.06	0.15 ± 0.06	0.28 ± 0.07	0.13 ± 0.05	4.8
	Zone-3	0.27 ± 0.02	0.13 ± 0.07	0.12 ± 0.04	0.56 ± 0.07	0.26 ± 0.08	4.6
	Zone-4	0.35 ± 0.02	0.14 ± 0.05	0.24 ± 0.05	0.63 ± 0.04	0.37 ± 0.06	−1.9
	Zone-5	0.41 ± 0.02	0.18 ± 0.04	0.31 ± 0.05	0.70 ± 0.02	0.45 ± 0.05	−0.5
OLR	South Asia	293.7 ± 0.6	287.6 ± 2.3	300.3 ± 2.1	294.1 ± 1.6	292.6 ± 1.7	−0.3
	Zone-1	326.3 ± 1.8	295.4 ± 6	332.2 ± 7.3	346.2 ± 6	331.3 ± 4.9	−0.4
	Zone-2	308.3 ± 2.1	290.2 ± 3.9	319.3 ± 7.2	309.8 ± 5.6	313.5 ± 5.2	−1.1
	Zone-3	310 ± 2.2	303.2 ± 5.3	331.7 ± 7.7	296.2 ± 5	308.5 ± 4.3	−1.6
	Zone-4	298.7 ± 1	303.3 ± 3.4	308.1 ± 4.7	286.7 ± 1.7	296.5 ± 3	−0.2
	Zone-5	295.1 ± 0.7	305.9 ± 2.9	304.1 ± 3.8	280.8 ± 1.1	289.9 ± 2.4	0.3
RH	South Asia	50.8 ± 1.3	47.6 ± 3.8	40.7 ± 4	61.9 ± 2.9	52.7 ± 2.8	4.3
	Zone-1	26.2 ± 1	32.5 ± 5.4	20.2 ± 3.4	27.5 ± 3.2	24.2 ± 3.3	0.2
	Zone-2	43.1 ± 1.9	41.7 ± 5.8	32.7 ± 6.2	54.6 ± 4.8	43.1 ± 4.9	8.8
	Zone-3	44.1 ± 1.8	42.5 ± 6.1	27.2 ± 5.6	58.1 ± 4.4	48.1 ± 4.4	9.6
	Zone-4	58.6 ± 1.4	48.9 ± 5	51.1 ± 4.6	71.1 ± 2.1	63.5 ± 3.2	1.2
	Zone-5	61.3 ± 0.9	51.5 ± 3.3	52.9 ± 3.3	72.3 ± 0.9	68.1 ± 1.3	0.7

Bangladesh including megacity Dhaka.

MACCity NO_x anthropogenic emissions show a phenomenal growth of 44%, averaged at $1.36 \pm 0.13 \times 10^{-11}$ kg m^{-2} s^{-1}, during the study period. Zone-3 has the highest average emission rates ($5.67 \pm 0.84 \times 10^{-11}$ kg m^{-2} s^{-1}) with 82% increase (Table 3).

MODIS-Aqua AOD shows an overall increase of 10.1% (*average*: 0.29 ± 0.01, *slope*: 0.003 and $r = 0.56$) in South Asian aerosols burden during 2005–2015. The rise in aerosols burden may be seen in conjunction with fast increase in urbanization, industrialization and agricultural practices. Meteorological factors such as humidity, precipitation, temperature, boundary layer height and wind speed drive aerosols seasonality (Ramachandran et al., 2012; Prasad et al., 2006; Dani et al., 2012; Alam et al., 2011). Crop residue and biomass burning, and transportation of aerosols also modulate aerosols concentrations over South Asia (Tariq et al., 2015, 2016; Tariq and Ali, 2015). The study zone-2 has the highest amount of aerosols burden showing mean value of AOD to be 0.5 ± 0.03 with a negative trend at − 0.9% during the study period. Increasing anthropogenic emissions from urban areas and coal based power plants have resulted in the highest increase of 33.6% in aerosols column over zone-4.

AIRS-Aqua temperature is found to be averaged at 295.9 ± 0.2 Kelvin (K) with the highest zonal value of 299.7 ± 0.3 K over zone-1. Some parts of the zone-1 consist of Sistan region located at the junction of Pakistan, Iran and Afghanistan borders. The climate of this zone is arid with evaporation exceeding about 4000 mm $year^{-1}$ as a result of high temperatures (Moghaddamnia et al., 2009; Rashki et al., 2012). GLDAS-NOAH wind speed is recoded to the highest level at 3.7 ± 0.1 m s^{-1} over zone-1 with the highest mean speed 4.3 ± 2.2 m s^{-1} in summer monsoon as a consequence of the strong northerlies (Levar or 120-days wind, Hossenzadeh, 1997) blowing in summer (Rashki et al.,

Table 4
Simple linear regression model equations representing tropo-NO_2 column ($\times 10^{15}$ molecules cm^{-2}) dependence on NO_x, AOD and meteorological factors for the five study zones and landmass of South Asia and adjoining region using monthly mean data during October 2004–December 2015. All correlations are significant at the 0.01 level (2–tailed) except numerals in bold which are significant at the 0.05 level. The regressors having high P-values (greater than 0.05) are excluded from the equations for more meaningful results.

	Simple linear regression equations	Correlation coefficient (r) or standardized regression coefficient (β)	Standard error
South Asia	$NO_2 = 0.685 + 1.420\ AOD$	0.56	0.11
	$NO_2 = 0.698 + 0.291\ NO_x$	0.40	0.12
	$NO_2 = 0.852 + 0.080\ WS$	0.24	0.13
	$NO_2 = 1.399 - 1.073\ Preci$	−0.63	0.13
	$NO_2 = 1.623 - 1.039\ CLF$	−0.62	0.13
Zone-1	$NO_2 = 0.721 + 0.005\ RH$	**0.19**	0.19
	$NO_2 = 0.986 - 0.724\ CLF$	−0.29	0.18
	$NO_2 = 1.578 - 0.199\ WS$	−0.58	0.15
	$NO_2 = 1.999 - 0.003\ OLR$	−0.41	0.17
	$NO_2 = 4.251 - 0.011\ Temp$	−0.45	0.17
	$NO_2 = 0.899 - 0.002\ Preci$	− **0.19**	0.19
	$NO_2 = 1.068 - 0.930\ AOD$	−0.41	0.17
Zone-2	$NO_2 = 2.921 - 0.014\ RH$	−0.41	0.38
	$NO_2 = 1.991 + 0.627\ AOD$	0.28	0.39
	$NO_2 = 2.563 - 1.395\ CLF$	−0.38	0.38
	$NO_2 = 8.344 - 0.020\ Temp$	−0.34	0.39
	$NO_2 = 2.469 - 0.004\ Preci$	−0.47	0.36
	$NO_2 = 1.601 + 0.128\ NO_x$	0.28	0.40
Zone-3	$NO_2 = 2.416 - 0.010\ RH$	−0.44	0.28
	$NO_2 = 1.437 + 1.229\ AOD$	0.53	0.26
	$NO_2 = 2.139 - 0.554\ CLF$	−0.39	0.28
	$NO_2 = -0.362 + 0.008\ OLR$	0.41	0.28
	$NO_2 = -1.648 + 0.012\ Temp$	0.21	0.30
	$NO_2 = 2.074 - 0.001\ Preci$	−0.38	0.29
	$NO_2 = 1.680 + 0.055\ NO_x$	**0.17**	0.31
Zone-4	$NO_2 = 3.668 - 0.032\ RH$	−0.81	0.26
	$NO_2 = 0.827 + 2.210\ AOD$	0.59	0.35
	$NO_2 = 2.357 - 1.614\ CLF$	−0.79	0.27
	$NO_2 = -8.557 + 0.035\ OLR$	0.80	0.26
	$NO_2 = 13.071 - 0.038\ Temp$	−0.29	0.41
	$NO_2 = 2.100 - 0.002\ Preci$	−0.74	0.29
	$NO_2 = 0.143 + 0.326\ NO_x$	0.65	0.33
Zone-5	$NO_2 = 3.518 - 0.042\ RH$	−0.79	0.36
	$NO_2 = 0.365 + 2.051\ AOD$	0.43	0.52
	$NO_2 = 1.565 - 1.529\ CLF$	−0.59	0.47
	$NO_2 = -9.334 + 0.035\ OLR$	0.73	0.39
	$NO_2 = -25.295 + 0.089\ Temp$	0.32	0.55
	$NO_2 = 1.245 - 0.002\ Preci$	−0.54	0.49
	$NO_2 = -1.260 + 1.190\ WS$	0.60	0.47
	$NO_2 = -2.090 + 6.097\ NO_x$	0.74	0.39

2012). The lowest annual mean wind speed $1.9 \pm 0.03\ m\ s^{-1}$ is observed over zone-5. TRMM precipitation annual mean 199.3 ± 16.4 mm per month, AIRS-Aqua retrieved relative humidity annual mean $61.3 \pm 0.9\%$ and AIRS-Aqua cloud fraction annual mean $0.41 \pm 0.02\%$ are observed to be the highest over zone-5. The seasonal peak values of $478.9 \pm 59.7\ mm\ month^{-1}$, $0.7 \pm 0.02\%$ and $72.3 \pm 0.9\%$ of these parameters are observed in summer monsoon respectively. The climate of this zone is described as tropical monsoon. AIRS outgoing long-wave radiation value is the highest 310 ± 2.2 over zone-3 with maximum value in pre-monsoon $331.7 \pm 7.7\ W\ m^{-2}$ followed by $308.5 \pm 4.3\ W\ m^{-2}$ in post-monsoon.

3.1. Modeling of OMI tropo-NO_2 column

Monthly mean values of tropo-NO_2, AOD and meteorological parameters have been used to model monthly mean tropo-NO_2 column over landmass of South Asia and five study zones (1–5), and to check its dependence on NO_x, AOD and meteorological parameters that largely affect the tropo-NO_2 concentration.

3.1.1. Simple linear regression modeling

Simple linear regression has been applied to different climatic zones and land use/land cover (LULC) types in South Asia, and the proposed models are given in Table 4. It is seen that tropo-NO_2 columns over different climatic zones and LULC types in South Asia are significantly dependent on NO_x, AOD and meteorological factors. Over landmass of South Asia, AOD, NO_x, WS, Preci, and CLF significantly participated in the models. All the selected meteorological factors and aerosols contributed significantly in the predicted models over zone-5 with the highest contribution from RH (β = − 0.79) followed by OLR (β = 0.73), whereas, the lowest contribution is from Temp (β = 0.32). From all the simple linear models, the highest value of β has been observed for RH (−0.81) followed by OLR (0.80) for zone-4. The lowest value of standard error is observed for AOD (0.11) while predicting tropo-NO_2 over South Asia. On the other hand, large values of standard errors are noted for Temp (0.55) and AOD (0.52) for zone-5.

To support our analysis, we have mapped spatial distribution of the correlations obtained for each grid point separated at 1° × 1° (Fig. 3). These maps would enable us to see spatial patterns of correlations for detailed analysis. For the computation of spatial correlations between tropo-NO_2 and NO_x, AOD and meteorological factors, monthly mean data have been used for each grid point. Significant correlations can be seen over Indus-Ganges Basin (IGB). IGB is attributed with high population density, industrialization and urbanization, and intense agricultural practices including large-scale crop-waste burning. High correlation of tropo-NO_2 and AOD is also observed over the eastern mining region of India. Sistan region (zone-1) shows significant correlation with a wide range of spatial correlations from $r = -0.20$ to $r = 0.66$. The lowest columns of tropo-NO_2 at 0.9 ± 0.03 ($\times 10^{15}$ molecules cm^{-2}) and AOD at 0.22 ± 0.02 are due to less human made emissions in this region linked to

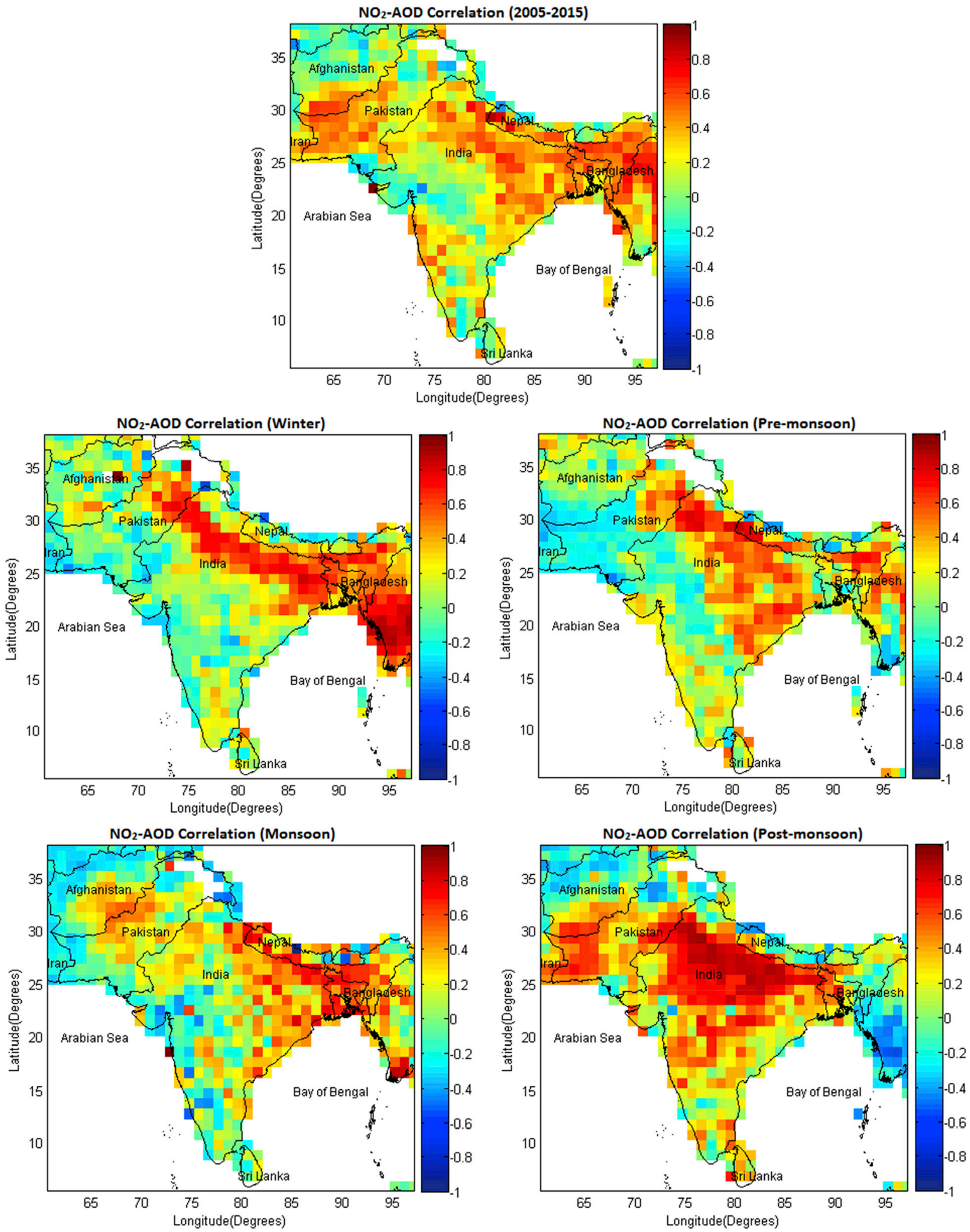

(a)

Fig. 3. Annual mean and seasonal spatial correlation maps of NO_2 ($\times 10^{15}$ molecules cm^{-2}) with (a) AOD (unit less), (b) temperature (K), (c) cloud fraction (%), (d) outgoing long-wave radiation (W m^{-2}), (e) precipitation rate (mm $month^{-1}$), (f) relative humidity (%), (g) surface wind speed (m s^{-1}) and (h) anthropogenic NO_x emissions (kg m^{-2} s^{-1}) for South Asia during October 2004–December 2015.

low population. Therefore high correlation indicates that the variability of tropo-NO_2 and AOD is largely determined by natural causes such as transported air pollutants and local meteorology. Average MACCity anthropogenic NO_x emissions show good spatial correlations with tropo-

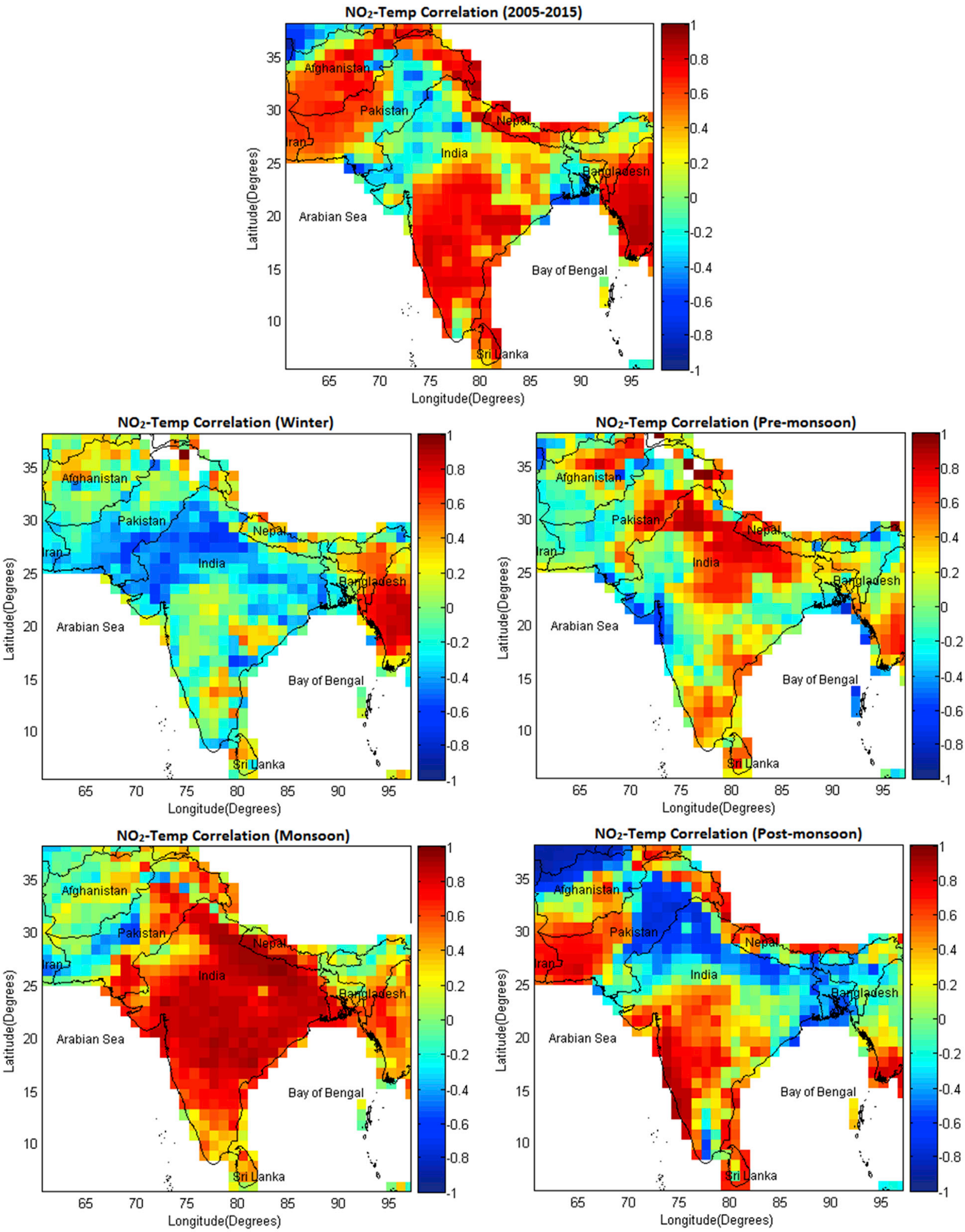

(b)

Fig. 3. (*continued*).

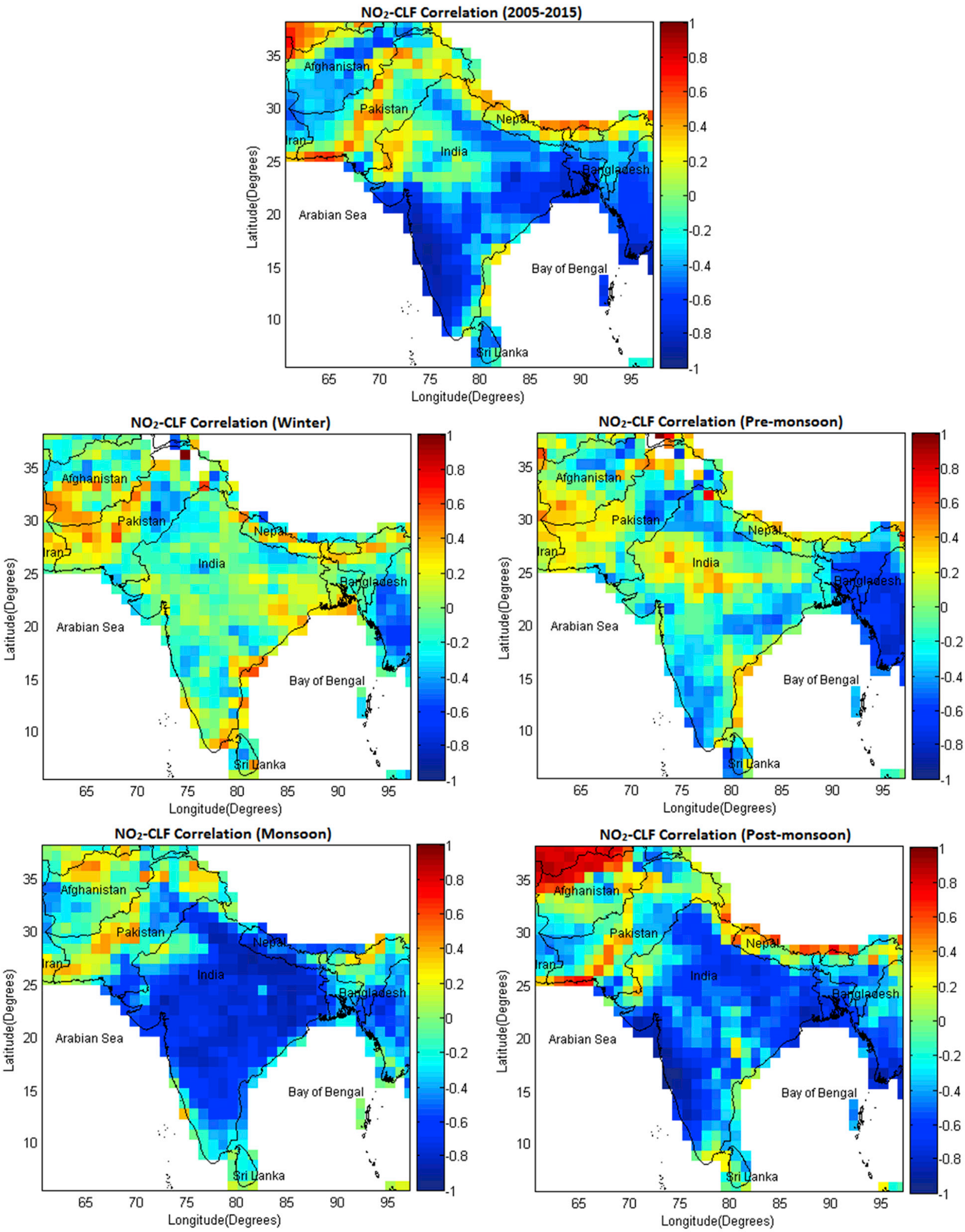

(c)

Fig. 3. (*continued*).

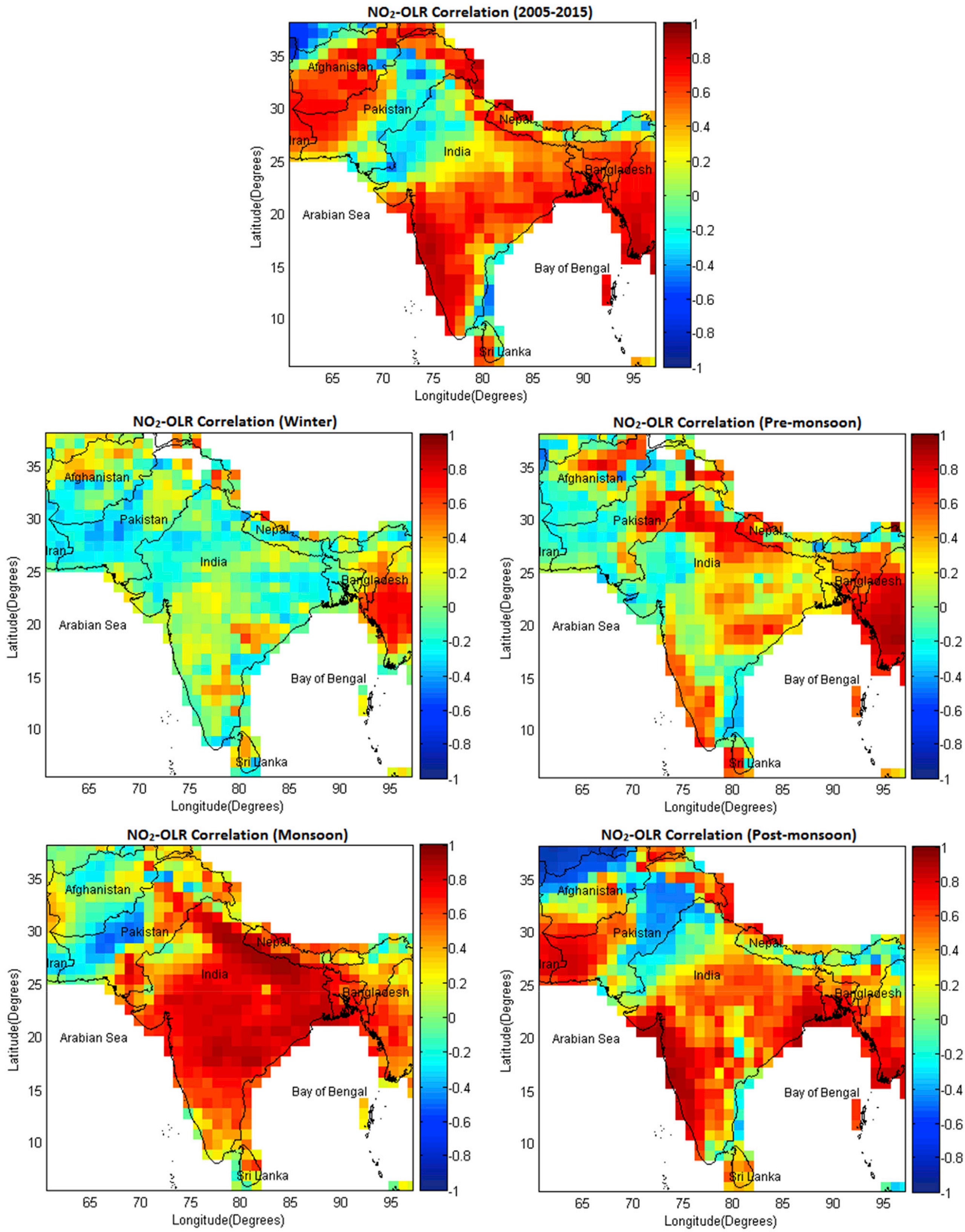

(*d*)

Fig. 3. (*continued*).

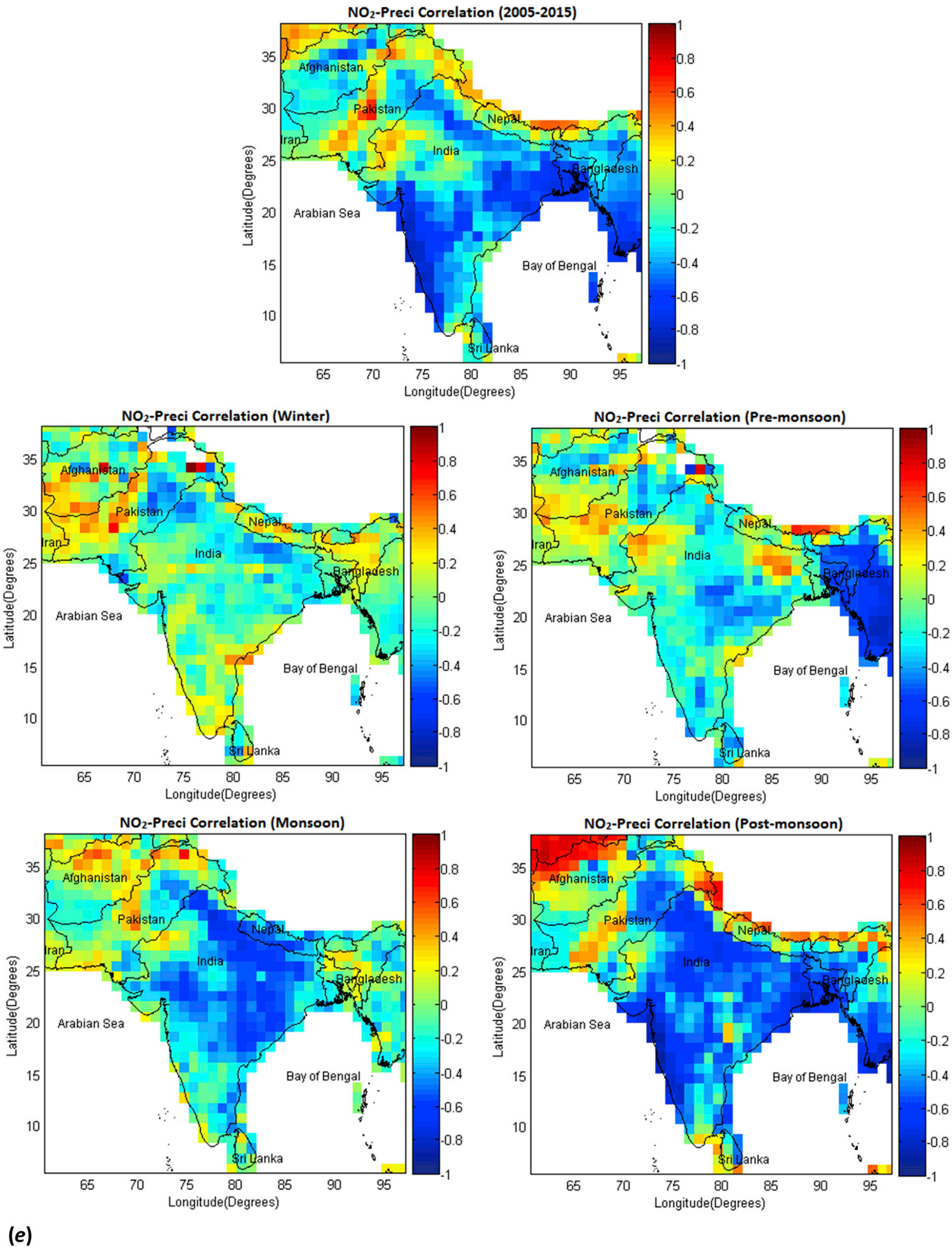

Fig. 3. (*continued*).

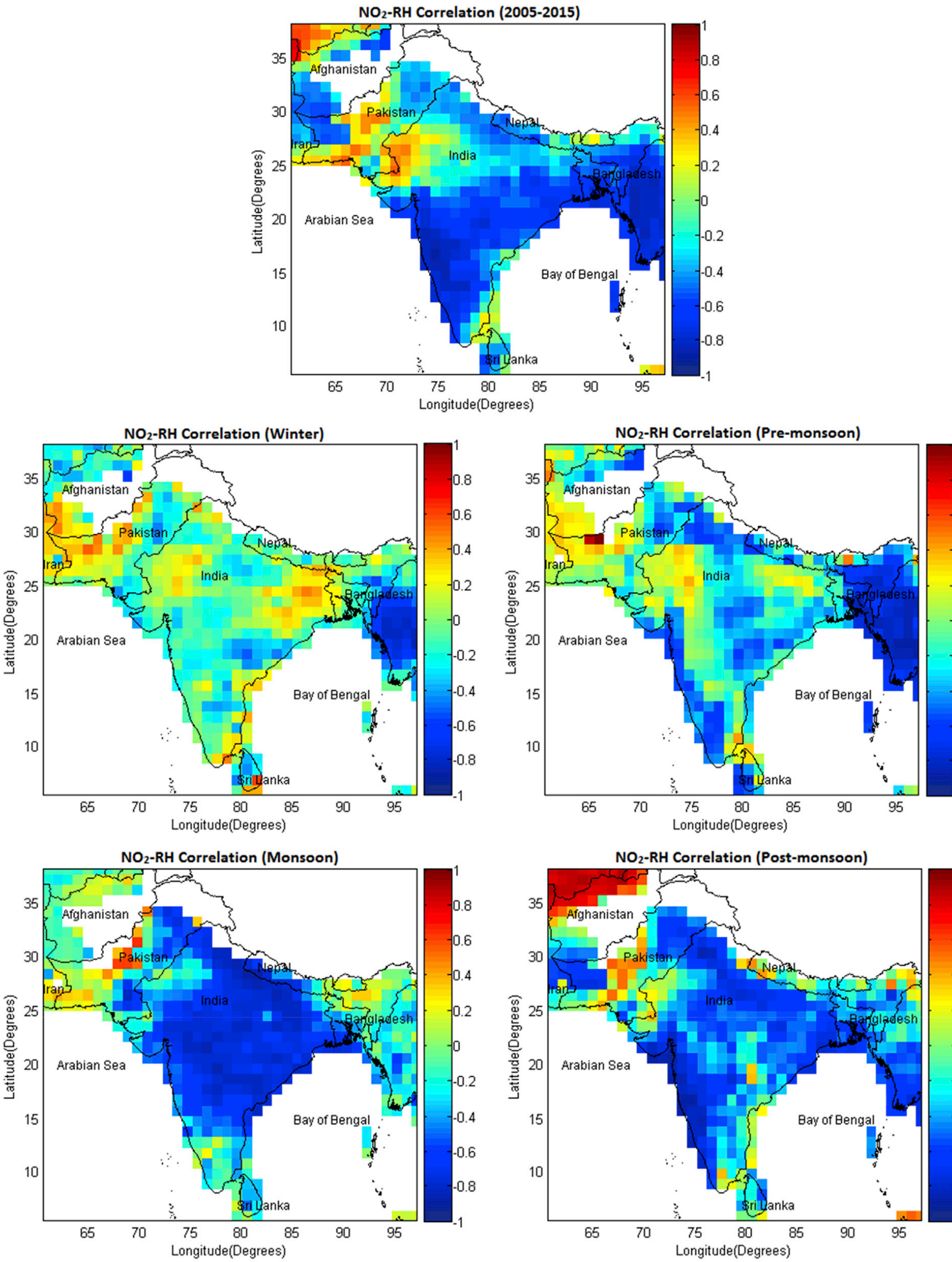

(f)

Fig. 3. (*continued*).

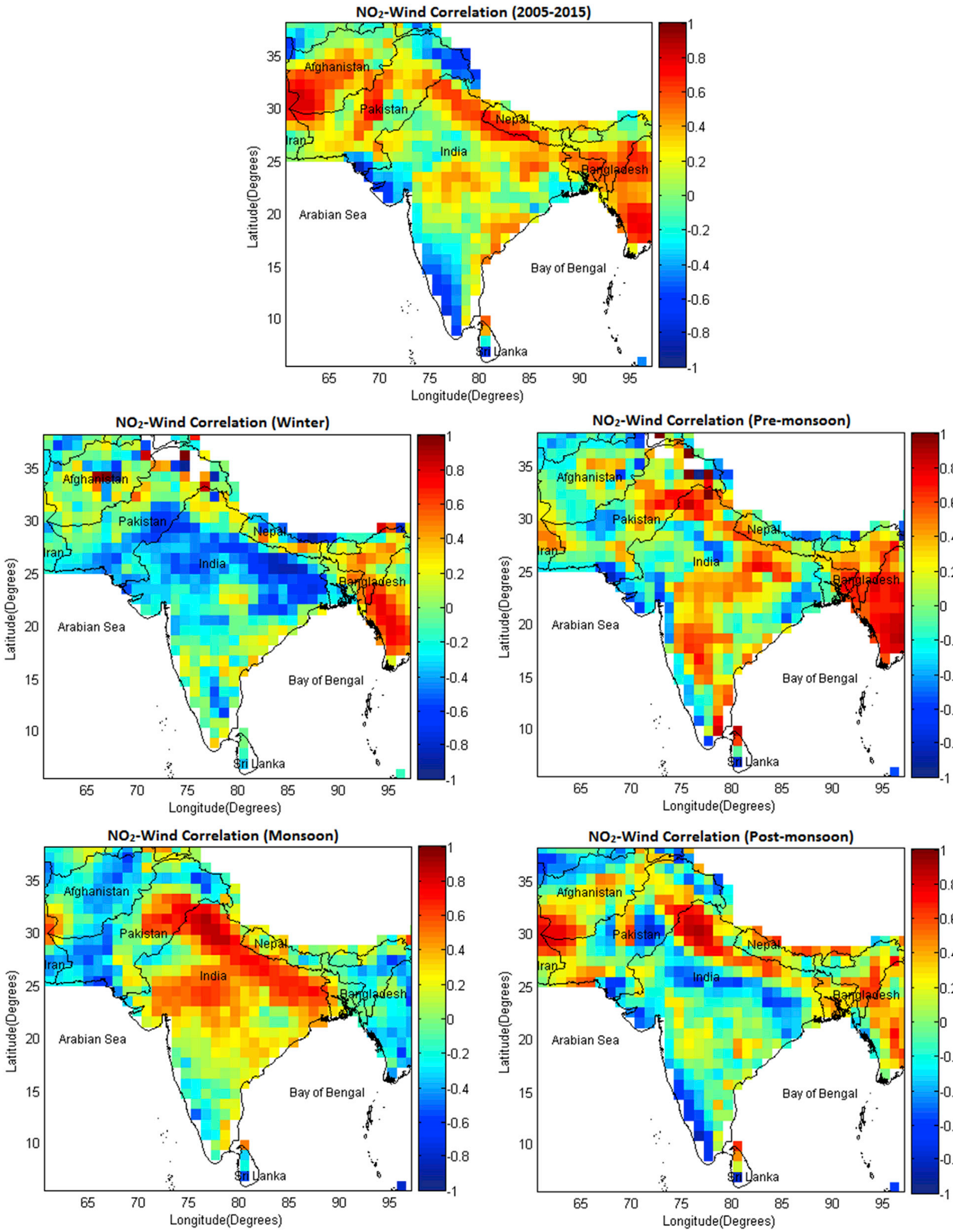

(g)

Fig. 3. (*continued*).

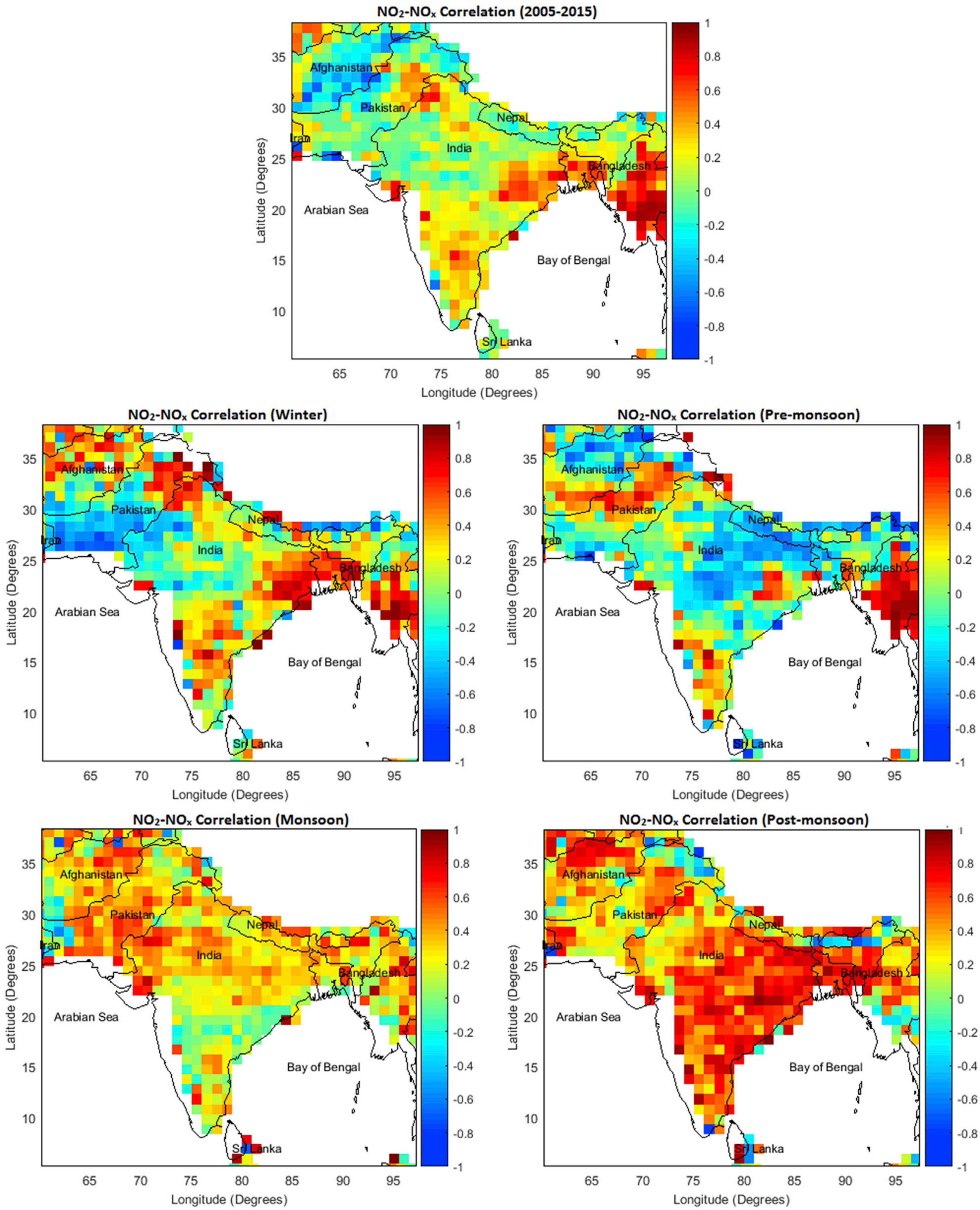

(*h*)

Fig. 3. (*continued*).

NO_2 in South Asia r ranging from −0.87 to 0.96. Zones 2–5 have shown good correlations linked to urban, agricultural, and industrialized areas. Enhanced positive correlations of tropo-NO_2 are found with Temp and OLR over the zones 2–5 in monsoon season. On the contrary, negative correlations have been found for CLF and RH, in monsoon season, over the same zones. The study zones 2–4 have shown positive correlation with WS in monsoon season. Preci has negative correlation with tropo-NO_2 over zones 2–5 in monsoon and post-monsoon seasons.

Table 5
The stepwise multiple linear regression models developed for tropo-NO_2 column ($\times 10^{15}$ molecules cm^{-2}) over landmass of South Asia and adjoining region, five study zones and some other selected areas using monthly mean data during October 2004–December 2015. All correlations are significant at the 0.01 level (2–tailed). The regressors having high P-values (greater than 0.05) are excluded from the equations for more meaningful results. The values in parentheses are Standardized Regression Coefficients (Beta, β) representing regressors's relative impacts.

	Stepwise regression model equations	Multiple r	Standard error
South Asia	$NO_2 = 0.882–0.007\ RH\ (-0.49) + 1.066\ AOD\ (0.422) + 0.177\ NO_x\ (0.247)$	0.82	0.08
Zone-1	$NO_2 = -2.962–0.016\ OLR\ (-1.848) + 0.032\ Temp\ (1.245) - 1.947\ CLF\ (-0.77) - 0.364\ AOD\ (0.161)$	0.69	0.14
Zone-2	$NO_2 = 1.494 + 1.12\ AOD\ (0.495) - 0.016\ RH\ (-0.461) + 0.173\ NO_x\ (0.378)$	0.66	0.31
Zone-3	$NO_2 = -9.881 + 0.046\ Temp\ (0.764) + 1.468\ AOD\ (0.628) - 0.872\ CLF\ (-0.615) - 0.007\ OLR\ (-0.381)$	0.76	0.20
Zone-4	$NO_2 = -4.451 + 0.019\ OLR\ (0.437) + 0.974\ AOD\ (0.261) + 0.114\ NO_x\ (0.226) - 0.008\ RH\ (-0.193)$	0.90	0.19
Zone-5	$NO_2 = -20.18–0.023\ RH\ (-0.424) + 1.306\ AOD\ (0.273) + 0.012\ OLR\ (0.245) + 1.916\ NO_x\ (0.231) + 0.06\ Temp\ (0.211)$	0.93	0.21
Karachi	$NO_2 = -0.399–0.054\ Temp\ (-0.448) + 0.089\ NO_x\ (0.411) + 0.011\ OLR\ (0.252) - 0.076\ WS\ (-0.224)$	0.84	0.24
Thar Desert	$NO_2 = 0.893 + 0.004\ RH\ (0.293) + 0.11\ AOD\ (0.183)$	0.37	0.16
Lahore	$NO_2 = 2.776 + 0.339\ NO_x\ (0.427) + 2.891\ AOD\ (0.419) - 0.043\ RH\ (-0.397) - 0.057\ Temp\ (-0.35)$	0.85	0.73
Delhi	$NO_2 = 8.44–0.11\ Temp\ (-0.562) + 1.997\ AOD\ (0.343) - 0.031\ RH\ (-0.269) - 1.59\ CLF\ (-0.195) - 1.809\ Preci\ (-0.142) + 0.032\ NO_x\ (0.088)$	0.92	0.60
Colombo	$NO_2 = 2.328–0.021\ RH\ (-0.582) + 0.267\ AOD\ (0.302)$	0.74	0.12
Kolkata	$NO_2 = -1.524–0.065\ Temp\ (-0.359) + 0.902\ AOD\ (0.297) - 0.656\ CLF\ (-0.23) + 0.018\ NO_x\ (0.13) - 0.004\ RH\ (-0.063) + 0.019\ OLR\ (0.26)$	0.91	0.28
Dhaka	$NO_2 = -5.935 + 0.548\ NO_x\ (0.593) - 0.676\ WS\ (-0.296) - 0.151\ Temp\ (-0.271) + 0.038\ OLR\ (0.228)$	0.94	0.55

3.1.2. Stepwise multiple linear regression modeling

The standardized regression coefficients (β) obtained from MLR analysis show significantly dependence of tropo-NO_2 on RH (β = − 0.49), AOD (β = 0.42) and NO_x (β = 0.25) for landmass of South Asia with strong correlation (r = 0.82) and standard error (of 0.08). The tropo-NO_2 column over zone-5 has the largest correlation (r = 0.93) and exhibited its greatest dependence on RH (β = − 0.42) followed by AOD (β = 0.27) (Table 5). Also AOD appears as a significant predictor of tropo-NO_2 in all the models for South Asia and study zones as presented in Table 5.

MLR is also applied on data for some of the large urban and important areas viz. megacity Lahore, megacity Delhi, coastal megacity Karachi, megacity Kolkata, megacity Dhaka, coastal city Colombo, and Thar Desert. We find a higher value of AOD β (of 0.42) for Lahore, located in warm semi arid zone-2 with large scale crop-residue burning, than the AOD β (of 0.34) for Delhi model indicating more influence of aerosols on the modeled tropo-NO_2 column for Lahore. The highest value of correlation coefficient for observed and modeled tropo-NO_2 is found for Dhaka (r = 0.94) with standard error of 0.55 (Table 5). Thar Desert located in the Pakistan and India borders shows the lowest correlation coefficient (r = 0.37) with standard error 0.16.

To evaluate the validity of the proposed models for the zones (1–5), bi-variate linear regression is applied to obtain the relationship between the observed tropo-NO_2 and the modeled tropo-NO_2 presented in Fig. 4. Overall, good agreements between the observed and modeled tropo-NO_2 values have been found and reflected by high correlation coefficients values. As revealed by the higher correlation coefficients (r), the multiple regressions reasonably model tropo-NO_2 over South Asia (r = 0.82), zone-4 (r = 0.90) and zone-5 (r = 0.93) (Fig. 4 and Table 5). The lowest zonal r = 0.66 has been found for zone-2 which has the largest amount of constant NO_2 emission sources such as industries, urban areas and power plants (Ghude et al., 2008; Badarinath et al., 2009).

The time series of observed and modeled tropo-NO_2 for South Asia and the study zones are presented in Fig. 4. Though, all the modeled time series fairly follow the observed variations of tropo-NO_2 columns with r ranging from 0.55 to 0.93, some big differences between the time series have been identified which are mostly linked to NO_2 enhancements due to pre- and post-monsoon crop-residue burning events largely occurring in zones 2–5. It is observed that post-monsoon rice residue burning significantly contributes in tropo-NO_2 columns over zone 2 and 3, and pre-monsoon wheat residue burning is a prominent source of tropo-NO_2 over zones 4 and 5 (Badarinath et al., 2006, 2009; Prasad et al., 2006; Ghude et al., 2008, 2009; Ali et al., 2014; Ramachandran et al., 2013; Renuka et al., 2014; ul-Haq et al., 2014, 2015, 2016, 2017).

Some anomalous results appear in Tables 4 and 5. It is well established that tropo-NO_2 is anti-correlated with temperature, relative humidity, precipitation and wind speed (Arya, 1999; Jones et al., 2010; Ramachandran et al., 2013). However positive beta weights have been found in the modeled equations for Temp (Table 4: zone-3 β = 0.21, zone-5 β = 0.32; Table 5: zone-1 β = 1.25, zone-3 β = 0.76, and zone-5 β = 0.21), RH (Table 4: zone-1 β = 0.19) and WS (Table 4: zone-5 β = 0.60). To understand the true effects of meteorological parameters on tropo-NO_2, multiple approaches are necessary. The nature and magnitude of these effects can vary from one geographical region to the other due to differences in the topographical features (Dawson et al., 2007; US EPA, 2009). Further, these parameters can affect NO_2 through direct physical mechanisms or indirectly through influences on other meteorological parameters (Ordonez et al., 2005; Jacob and Winner, 2009).

Here we discuss possible explanations for some of these anomalies. Zone-1 has low tropo-NO_2 (average $0.9 \pm 0.03 \times 10^{15}$ molecules cm^{-2}), low relative humidity (average 26.2 ± 1%), and high temperature (average 299.7 ± 0.3 K). Low relative humidity and less concentrations of dominant sources of hydroxyl radical (OH) limit the oxidation process of NO_2. Therefore, high temperatures with less relative humidity and hydroxyl radical (OH) are the probable reason for positive relations of Temp (β = 1.25) and RH (β = 0.19) with tropo-NO_2 over zone-1. In the central parts of Ganges Basin (zone-3), the increased energy demand for domestic and commercial purposes in pre-monsoon and monsoon seasons is mostly fulfilled by fossil fuel power plants contributing enhancements in NO_2 levels as evident from direct relation between temperature and NO_2. Kunhikrishnan et al. (2004) showed the existence of strong winds at 850 hPa during the summer monsoon directed from highly polluted central region of peninsular India to the region where zone-5 is located. This may be the reason for positive relation between tropo-NO_2 and WS for zone-5 (Table 4). Also seasonal high tropo-NO_2 1.73 ± 0.07 ($\times 10^{15}$ molecules cm^{-2}), due to pre monsoon crop residue burning, and high temperature 298.2 ± 0.6 K in pre-monsoon (Table 3) are the associated causes of direct relation between them.

For South Asia, a large disparity in the time series is found for March 2011 (Fig. 4). The observed large peak in March 2011 is due to intense pre-monsoon wheat residue burning events in the study zones 4 and 5 (shown in Fig. 5 *a-b*), which is not seen in the modeled time series. Fig. 5 (*a-d*) shows tropo-NO_2 and monthly mean active fire pixels (MCD14ML, Collection-6, at 1 km × 1 km grid) obtained from MODIS sensors onboard Aqua and Terra satellites available at http://firms.modaps.eosdis.nasa.gov/firemap/. The time series for zone-2 shows large differences in the both positive and negative peaks. The observed positive peaks are largely associated with wintertime enhancements and intense post-monsoon open field rice residue burning (Fig. 5 *c-d*). The post-monsoon dips are mostly due to strong winds observed in the zone. The modeled time series

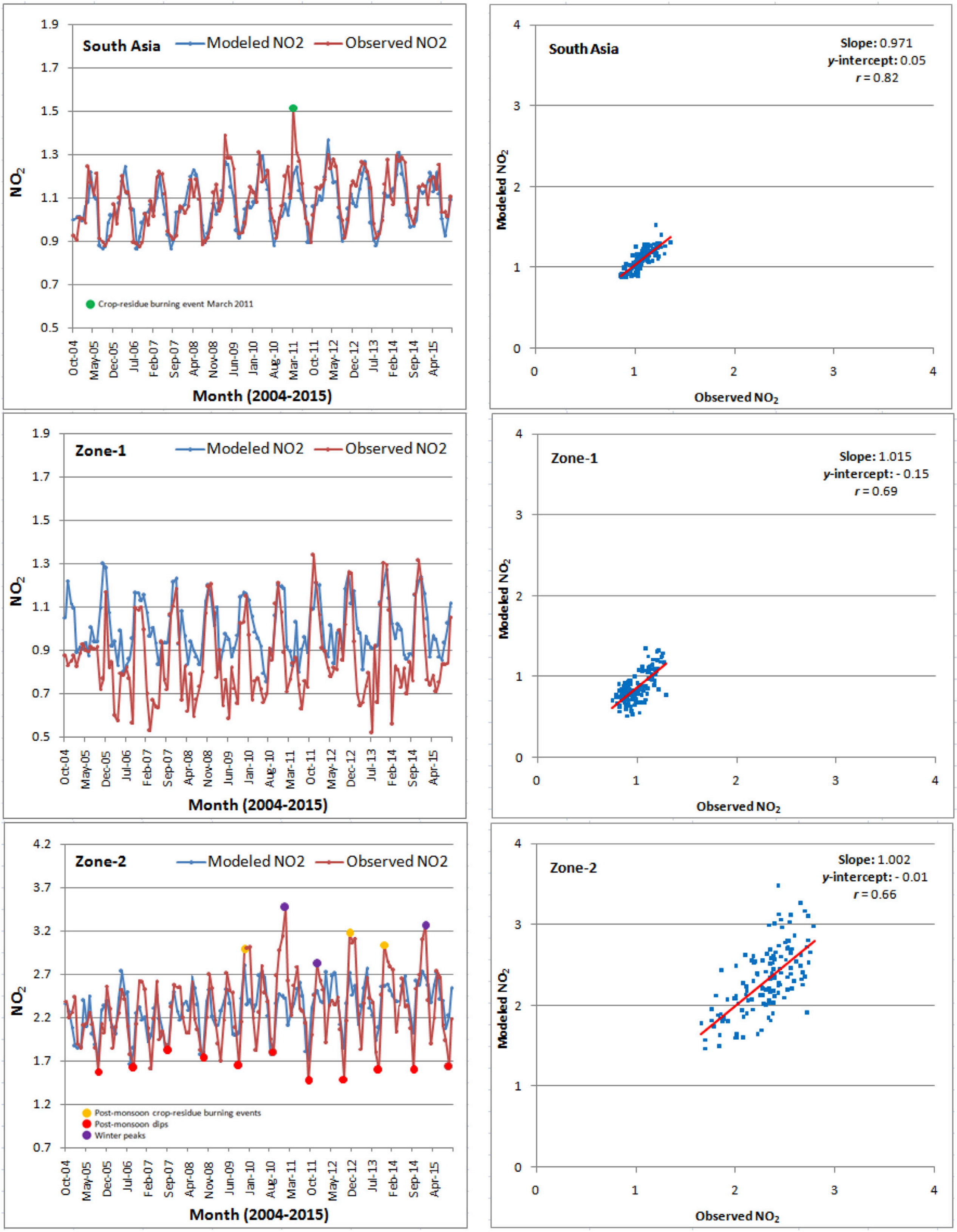

Fig. 4. The time series and scatter plots of observed and modeled tropo-NO_2 ($\times 10^{15}$ molecules cm^{-2}) over South Asia and the study zones during October 2004–December 2015.

for zones 4 and 5 have fairly matching dips of tropo-NO_2. On the contrary, large positive peaks are observed for tropo-NO_2 due to pre-monsoon wheat residue burning events causing the primary difference in the time series for the study zones 4 and 5. The effects of crop-residue burning on tropo-NO_2 time series for zones 2 and 3 are not as prominent as for zones 4 and 5 due to two reasons. Firstly, zones 2 and 3 are very

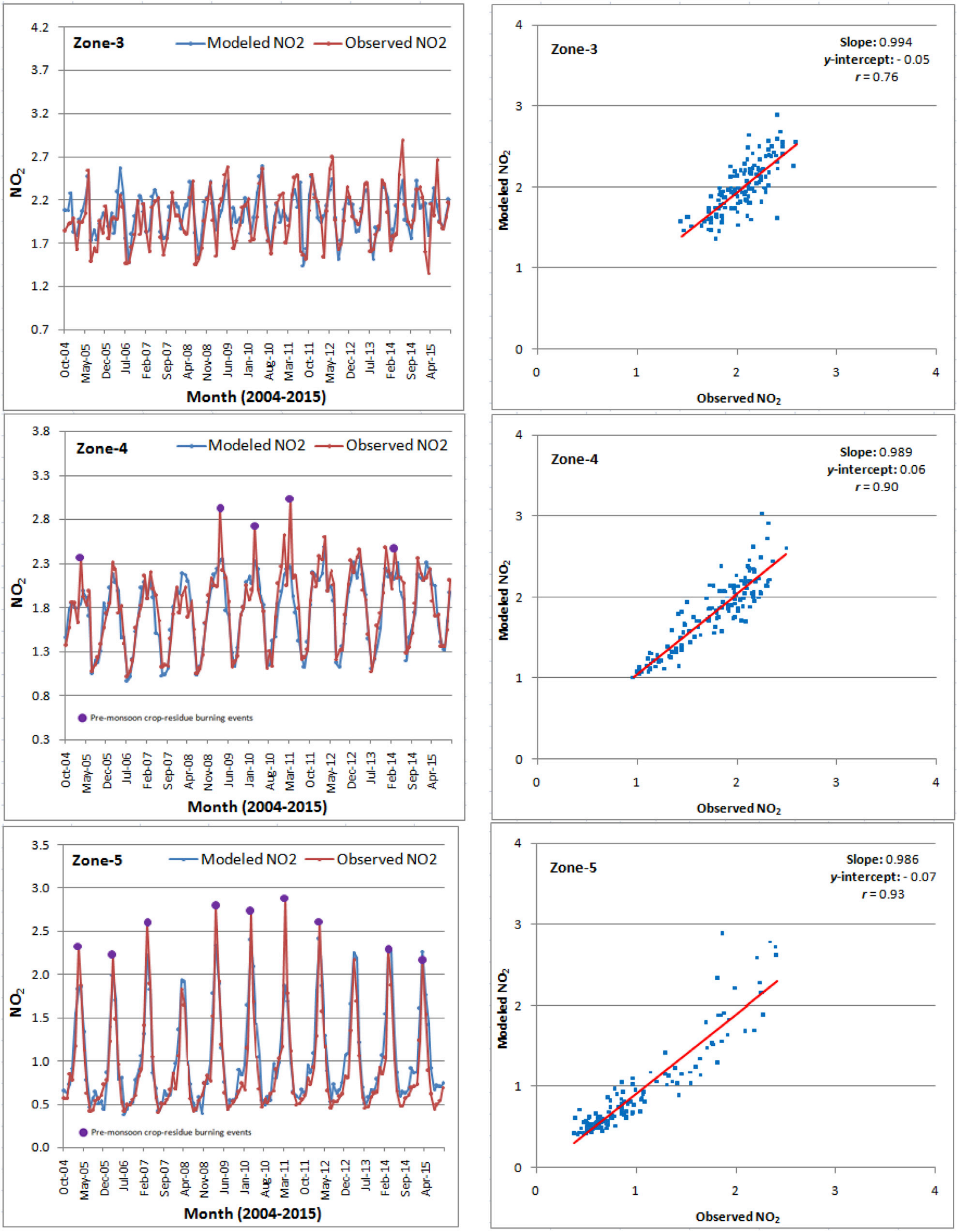

Fig. 4. (*continued*).

densely populated regions with large and steady emissions from urban areas, industries and power plants reflected by their average values. Zone-2 has the highest tropo-NO_2 averaged at 2.5 ± 0.12 ($\times 10^{15}$ molecules cm^{-2}) followed by zone-3 averaged at 2.03 ± 0.07 ($\times 10^{15}$ molecules cm^{-2}). Secondly, pre-monsoon crop residue burning from wheat fields (in zones 4 and 5) is more widespread and intense as compared to post-monsoon burning from rice fields (in zones 2 and 3) (Fig. 5b and d).

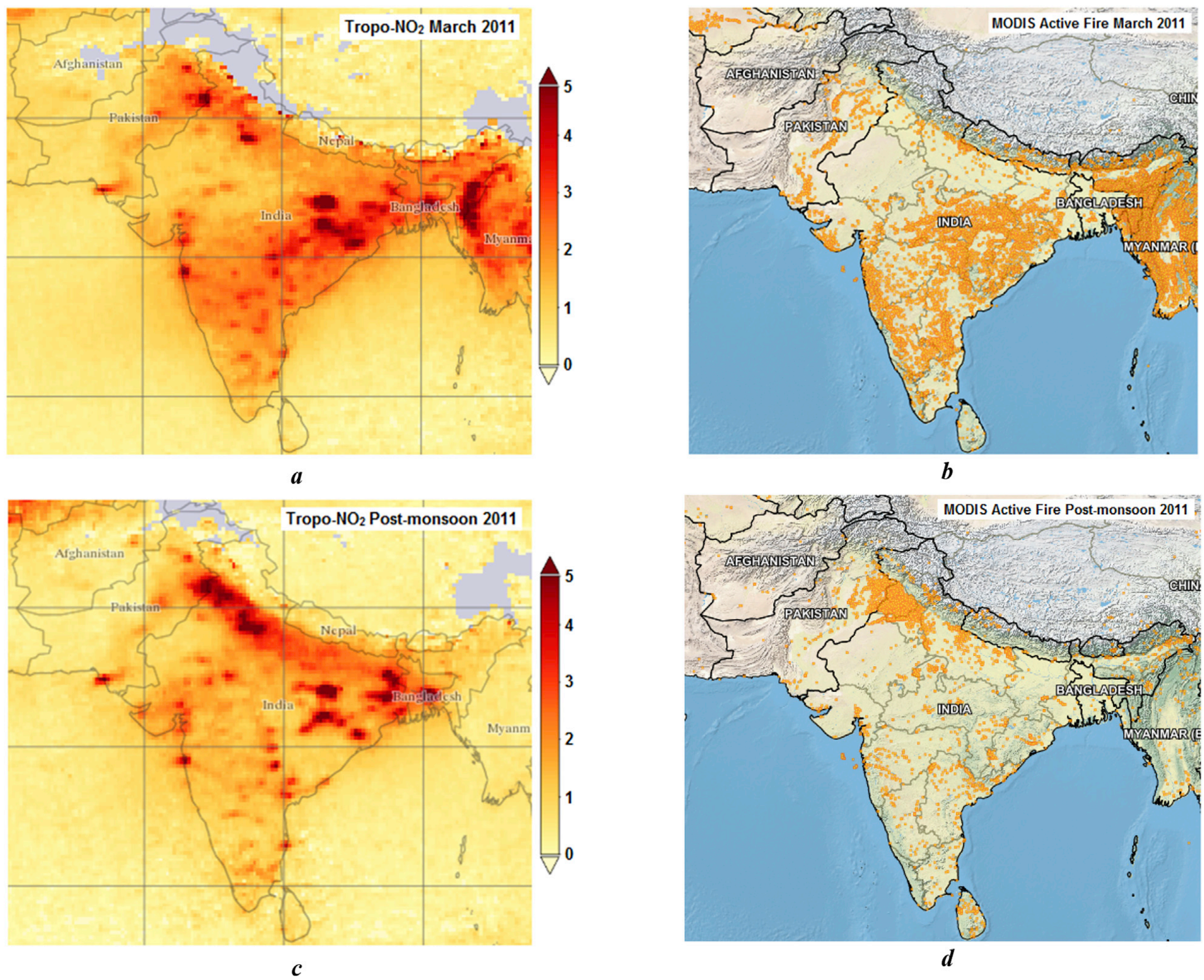

Fig. 5. Maps of OMI observed tropo-NO_2 ($\times 10^{15}$ molecules cm^{-2}) (panels a and c) and MODIS active fire pixels (panels b and d) during March 2011 (panels a and b), and post-monsoon 2011 (panels c and d) in South Asia.

4. Conclusion

Simple and multiple regression techniques have been applied to model tropo-NO_2 columns over landmass of South Asia, five study zones and some important urban and desert areas during the last decade from 2004 to 2015. The regressors of these analyses are NO_x, AOD, RH, Preci, Temp, CLF, WS and OLR. Our analyses show significant dependence of tropo-NO_2 on these factors. For bi-variate regression analysis, it is found that all the selected meteorological parameters have significantly contributed to the modeled tropo-NO_2 over eastern India and Myanmar (zone-5) with the highest contribution from RH ($\beta = -0.79$) followed by NO_x ($\beta = 0.74$), whereas, the lowest contribution is observed from Temp ($\beta = 0.32$). The large values of multiple r have been observed for RH (-0.81) and OLR (0.80) for eastern mining region of India and western Bangladesh (zone-4). Multiple linear regression shows that tropo-NO_2 variability is associated with NO_x, AOD, temperature, precipitation, relative humidity, cloud fraction and outgoing long wave radiation, being the main factors that control NO_2 seasonality. Excellent agreements are observed between the OMI retrieved and modeled tropo-NO_2 values. It is revealed that the multiple regression models reasonably predict tropo-NO_2 variations over the landmass of South Asia ($r = 0.82$), zone-4 ($r = 0.90$) and zone-5 ($r = 0.93$). Northwestern Indus-Ganges Basin (zone-2) shows the lowest r = 0.66 linked to the largest amount of constant NO_2 emission sources from industries and urban areas. Some large discrepancies have been noted between the observed and modeled tropo-NO_2 monthly mean time series for zones 2, 4 and 5 mostly related to pre- and post-monsoon crop-residue events. Some important urban areas located in different climatic zones and Thar Desert are also included in the analyses. We have found higher contribution of AOD ($\beta = 0.42$) in modeled tropo-NO_2 over Lahore compared to tropo-NO_2 over Delhi ($\beta = 0.34$) due to larger crop residue burning in the neighboring areas of Lahore. Detailed analysis of discrepancies found between tropo-NO_2 and different meteorological parameters over different locations is recommended for future research work.

Acknowledgements

We greatly acknowledge OMI, TRMM, AIRS, MODIS, GLDAS_NOAH, and MACCity project teams for providing data. We thank the editor and anonymous reviewers for their constructive and valuable suggestions which have greatly improved the quality of this paper.

References

Alam, K., Qureshi, S., Blaschke, T., 2011. Monitoring spatio-temporal aerosol patterns over Pakistan based on MODIS, TOMS and MISR satellite data and a HYSLPIT model. Atmos. Environ. 45, 4641–4651.

Ali, M., Tariq, S., Mahmood, K., Rana, A.D., Batool, A., ul-Haq, Z., 2014. A study of aerosol properties over Lahore (Pakistan) by using AERONET data. Asia-Pacific J. Atmos. Sci. 50, 153–162. https://doi.org/10.1007/s13143-014-0004-y.

Aron, A., Coups, E.J., Aron, E.N., 2013. Statistics for Psychology, sixth ed. Pearson, NJ (USA), p. 819.

Arya, P.S., 1999. Air Pollution Meteorology and Dispersion. Oxford University Press, New York.

Aumann, H.H., Chahine, M.T., Gautier, C., Goldberg, M.D., Kalnay, E., McMillin, L.M., Revercomb, H., Rosenkranz, P.W., Smith, W.L., Staelin, D.H., Strow, L.L., Susskind, J., 2003. AIRS/AMSU/HSB on the aqua mission: design, science objectives, data products, and processing systems. IEEE Trans. Geosci. Rem. Sens. 41, 253–264.

Azad, A.K., Kitada, T., 1998. Characteristics of the air pollution in the city of Dhaka, Bangladesh in winter. Atmos. Environ. 32 (11), 1991–2005.

Badarinath, K.V.S., Kiran Chand, T.R., Krishna Prasad, V., 2006. Agriculture crop residue burning in the Indo-Gangetic Plains—a study using IRS-P6 AWiFS satellite data. Curr. Sci. 91, 1085–1089.

Badarinath, K.V.S., Kharol, S.K., Sharma, A.R., Prasad, V.K., 2009. Analysis of aerosol and carbon monoxide characteristics over Arabian Sea during crop residue burning period in the Indo-Gangetic Plains using multi-satellite remote sensing datasets. J. Atmos. Sol. Terr. Phys. 71, 1267–1276.

Barck, C., Lundahl, J., Halldén, G., Bylin, G., 2005. Brief exposures to NO_2 augment the allergic inflammation in asthmatics. Environ. Res. 97, 58–66.

Bucsela, E.J., Celarier, E.A., Wenig, M.O., Gleason, J.F., Veefkind, J.P., Boersma, K.F., Brinksma, E.J., 2006. Algorithm for NO_2 vertical column retrieval from the ozone monitoring instrument. IEEE Trans. Geosci. Rem. Sens. 44, 1245–1258.

Bucsela, E.J., Krotkov, N.A., Celarier, E.A., Lamsal, L.N., Swartz, W.H., Bhartia, P.K., Boersma, K.F., Veefkind, J.P., Gleason, J.F., Pickering, K.E., 2013. A new stratospheric and tropospheric NO_2 retrieval algorithm for nadir–viewing satellite instruments: applications to OMI. Atmos. Meas. Tech. 6, 2607–2626.

Bucsela, E.J., Perring, A.E., Cohen, R.C., Boersma, K.F., Celarier, E.J., Gleason, J.F., Wenig, M.O., Bertram, T.H., Wooldrige, P.J., Dirksen, R., Veefkind, J.P., 2008. Comparison of NO2 in situ aircraft measurements with data from the ozone monitoring instrument. J. Geophys. Res. 113, D16S31 https://doi.org/10.1029/2007JD008838.

Case, G.D., Dixon, J.S., Schooley, J.C., 1979. Interactions of blood metalloproteins with nitrogen oxides and oxidant air pollutants. Environ. Res. 20, 43–65.

Celarier, E.A., Celarier, E.A., Brinksma, E.J., Gleason, J.F., Veefkind, J.P., Cede, A., Herman, J.R., Ionov, D., Goutail, F., Pommereau, J.-P., Lambert, J.-C., van Roozendael, M., Pinardi, G., Wittrock, F., Schönhardt, A., Richter, A., Ibrahim, O.W., Wagner, T., Bojkov, B., Mount, G., Spinei, E., Chen, C.M., Pongetti, T.J., Sander, S.P., Bucsela, E.J., Wenig, M.O., Swart, D.P.J., Volten, H., Kroon, M., Levelt, P.F., 2008. Validation of ozone monitoring instrument nitrogen dioxide columns. J. Geophys. Res. 113 (2008), D15S15. https://doi.org/10.1029/2007JD008908.

Cheng, M.M., Jiang, H., Guo, Z., 2012. Evaluation of long–term tropospheric NO2 columns and the effect of different ecosystem in Yangtze River Delta. Procedia Environ. Sci. 13, 1045–1056.

Clapp, L.J., Jenkin, M.E., 2001. Analysis of the relationship between ambient levels of O3, NO2 and NO as a function of NOx in the UK. Atmos. Environ. 35, 6391–6405.

Dancey, C., Reidy, J., 2014. Statistics without Maths for Psychology, sixth ed. Pearson Education Ltd., p. 640

Dani, K.K., Raj, P.E., Devara, P.C.S., Pandithurai, G., Sonbawne, S.M., Maheskumar, R.S., Saha, S.K., Rao, Y.J., 2012. Long-term trends and variability in measured multi-spectral aerosol optical depth over a tropical urban station in India. Int. J. Climatol. 32, 153–160.

David, L.M., Nair, P.R., 2013. Tropospheric column O3and NO2over the Indian region observed by Ozone Monitoring Instrument (OMI): seasonal changes and long-term trends. Atmos. Environ. 65, 25–39.

Demuzere, M., van Lipzig, N.P.M., 2010. A new method to estimate air-quality levels using a synoptic-regression approach. Part I: present-day O_3 and PM_{10} analysis. Atmos. Environ. 44, 1341–1355.

Dawson, J.P., Adams, P.J., Pandis, S.N., 2007. Sensitivity of ozone to summertime climate in the Eastern USA: a modeling case study. Atmos. Environ. 41, 1494–1511.

Engel-Cox, J.A., Holloman, C.H., Coutant, B.W., Hoff, R.M., 2004. Qualitative and quantitative evaluation of MODIS satellite sensor data for regional and urban scale air quality. Atmos. Environ. 38 (16), 2495–2509.

Fang, H., Beaudoing, Hiroko K., Rodell, Matthew, Teng, William L., Vollmer, Bruce E., 2009. Global land data assimilation system (GLDAS) products, services and application from NASA hydrology data and information services center (HDISC). In: ASPRS 2009 Annual Conference Baltimore, Maryland Š March 8-13, 2009.

Ferm, M., De Santis, F., Varotsos, C., 2005. Nitric acid measurements in connection with corrosion studies. Atmos. Environ. 39, 6664–6672. https://doi.org/10.1016/j.atmosenv.2005.07.044.

Ghose, M.K., Paul, R., Banerjee, S.K., 2004. Assessment of the Impacts of Vehicular Emissions on Urban Air Quality and its Management in Indian Context: the Case of Kolkata, vol. 7. Environmental Science and Policy, Calcutta, pp. 345–351.

Ghude, S.D., Fadnavis, S., Beig, G., Polade, S.D., van der A, R.J., 2008. Detection of surface emission hot spots, trends, and seasonal cycle from satellite-retrieved NO2 over India. J. Geophys. Res. Atmos. 113, D20305 https://doi.org/10.1029/2007JD009615.

Ghude, S.D., Van der A, R.J., Beig, G., Fadnavis, S., Polade, S.D., 2009. Satellite derived trends in NO_2 over the major global hotspot regions during the past decade and their intercomparison. Environ. Pollut. 157, 1873–1878.

Giovanni, 2016. Geospatial Interactive Online Visualization and Analysis Infrastructure. http://giovanni.gsfc.nasa.gov/giovanni/.

Granier, C., Bessagnet, B., Bond, T., D'Angiola, A., van der Gon, D.H., Frost, G.J., Heil, A., et al., 2011. Evolution of anthropogenic and biomass burning emissions of air pollutants at global and regional scales during the 1980-2010 period. Climatic Change 109 (1–2), 163–190. https://doi.org/10.1007/s10584-011-0154-1.

Gurjar, B.R., Butler, T.M., Lawrence, M.G., Lelieveld, J., 2008. Evaluation of emissions and air quality in megacities. Atmos. Environ. 42, 1593–1606.

Hallquist, M., et al., 2009. The formation, properties and impact of secondary organic aerosol: current and emerging issues. Atmos. Chem. Phys. 9 (14), 5155–5236.

Han, S.Q., Bian, H., Feng, Y.C., Liu, A.X., Li, X.J., Zeng, F., Zhang, X.L., 2011. Analysis of the relationship between O3, NO and NO2 in Tianjin, China. Aeros. Air Qual. Res. 11, 128–139.

Hossenzadeh, S.R., 1997. One hundred and twenty days winds of Sistan, Iran. J. Res. Geogr. 46, 103–127.

Jacob, D.J., Winner, D.A., 2009. Effect of climate change on air quality. Atmos. Environ. 43 (1), 51–63.

Jones, A.M., Harrison, R.M., Baker, J., 2010. The wind speed dependence of the concentrations of airborne particulate matter and NO_X. Atmos. Environ. 44, 1682–1690.

Joshi, R.M., 2015. Education in South Asia. In: International Encyclopedia of the Social & Behavioral Sciences, second ed., pp. 194–197.

Kanaya, Y., Tanimoto, H., Matsumoto, J., Furutani, H., Hashimoto, S., Komazaki, Y., Tanaka, S., Yokouchi, Y., Kato, S., Kajii, Y., Akimoto, H., 2007. Diurnal variations in H_2O_2, O_3, PAN, HNO_3 and aldehyde concentrations and NO/NO_2 ratios at Rishiri Island, Japan: potential influence from iodine chemistry. Sci. Total Environ. 376, 185–197.

Kaufman, Y.J., Tanre, D., Remer, L.A., Vermote, E.F., Che, A., Holben, B.N., 1997. Operational remote sensing of tropospheric aerosol over land from EOS moderate resolution imaging spectroradiometer. J. Geophys. Res. 102, 17051–17067.

Kondratyev, K.Y., Varotsos, C.A., 2001. Global tropospheric ozone dynamics Part I: tropospheric ozone precursors Part II: numerical modelling of tropospheric ozone variability. Environ. Sci. Pollut. Res. 8, 57. https://doi.org/10.1007/BF02987295.

Kottek, M., Grieser, J., Beck, C., Rudolf, B., Rubel, F., 2006. World Map of the Köppen-Geiger climate classification updated. Meteorol. Z. 15 (3), 259–263. https://doi.org/10.1127/0941-2948/2006/0130.

Kroll, J.H., Seinfeld, J.H., 2008. Chemistry of secondary organic aerosol: formation and evolution of low-volatility organics in the atmosphere. Atmos. Environ. 42 (16), 3593–3624.

Kunhikrishnan, T., Lawrence, M.G., von Kuhlmann, R., Richter, A., Ladstätter-Weissenmayer, A., Burrows, J.P., 2004. Analysis of tropospheric NOx over Asia using the model of atmospheric transport and chemistry (MATCH-MPIC) and GOME-satellite observations. Atmos. Environ. 38, 581–596. https://doi.org/10.1016/j.atmosenv.2003.09.074.

Levelt, P.F., van den Oord, G.H.J., Dobber, M.R., Malkki, A., Visser, H., de Vries, J., Stammes, P., Lundell, J.O.V., Saari, H., 2006. The ozone monitoring instrument. IEEE Trans. Geosci. Rem. Sens. 44 (5).

Li, A., Zhao, W., Deng, W., 2015. A quantitative inspection on spatio-temporal variation of remote sensing-based estimates of land surface evapotranspiration in South Asia. Rem. Sens. 7 (4), 4726–4752.

Lin, M., Tao, J., Chan, C.-Y., Cao, J.-J., Zhang, Z.-S., Zhu, L.-H., Zhang, R.-J., 2012. Regression analyses between recent air quality and visibility changes in megacities at four haze regions in China. Aerosol Air Qual. Res. 12, 1049–1061. https://doi.org/10.4209/aaqr.2011.11.0220.

Liu, Z., Ostrenga, Dana, Teng, William, Kempler, Steven, 2012. Tropical Rainfall measuring mission (TRMM) precipitation data and services for research and applications. Am. Meteorol. Soc. BAMS 1317–1325.

Moghaddamnia, A., Ghafari, M.B., Piri, J., Amin, S., Han, D., 2009. Evaporation estimation using artificial neural networks and adaptive neuro-fuzzy inference system techniques. Adv. Water Resour. 32, 88–97.

OMI, 2012. OMI Data User's Guide available at: https://docserver.gesdisc.eosdis.nasa.gov/repository/Mission/OMI/3.3_ScienceDataProductDocumentation/3.3.2_ProductRequirements_Designs/README.OMI_DUG.pdf.

Ordonez, C., Mathis, H., Furger, M., Henne, S., Hoglin, C., Staehelin, J., Prevot, A.S.H., 2005. Changes of daily surface ozone maxima in Switzerland in all seasons from 1992 to 2002 and discussion of summer 2003. Atmos. Chem. Phys. 5, 1187–1203.

Pagano, T.S., Aumann, H.H., Hagan, D.E., Overoye, K., 2003. Prelaunch and in-flight radiometric calibration of the atmospheric infrared sounder (AIRS). IEEE Trans. Geosci. Rem. Sens. 41 (2), 265–273.

Parra, M.A., Elustondo, D., Bermejo, R., Santamaria, J.M., 2009. Ambient air levels of volatile organic compounds (VOC) and nitrogen dioxide (NO_2) in a medium size city in Northern Spain. Sci. Total Environ. 407, 999–1009.

Prasad, A.K., Singh, R.P., Singh, A., 2006. A seasonal climatology of aerosol optical depth over the Indian subcontinent: trend and departures in recent years. Int. J. Rem. Sens. 27 (12), 2323–2329.

Ramachandran, S., Kedia, S., Srivastava, R., 2012. Aerosol optical depth trends over different regions of India. Atmos. Environ. 49, 338–347.

Ramachandran, A., Jain, N.K., Sharma, S.A., Pallipad, J., 2013. Recent trends in tropospheric NO_2 over India observed by SCIAMACHY: identification of hot spots. Atmos. Pollut. Res. 4, 354–361.

Rashki, A., Kaskaoutis, D.G., deW Rautenbach, C.J., Eriksson, P.G., Qiang, M., Gupta, P., 2012. Dust storms and their horizontal dust loading in the Sistan region, Iran. Aeolian Res. 5, 51–62.

Renuka, K., Gadhavi, H., Jayaraman, A., Lal, S., Naja, M., Rao, S.V.B., 2014. Study of ozone and NO2 over Gadanki—a rural site in South India. J. Atmos. Chem. 71, 95–112.

Richter, A., Burrows, J.P., 2002. Tropospheric NO_2 from GOME measurements. Adv. Space Res. 29, 1673–1683.

Salomonson, V.V., Barnes, W.L., Maymon, P.W., Montgomery, H.E., Ostrow, H., 1989. MODIS: Advanced facility instrument for studies of the Earth as a system. IEEE Trans. Geosci. Rem. Sens. 27, 145–153.

Seinfeld, J.H., Pandis, S.N., 1998. Atmospheric Chemistry and Physics—from Air Pollution to Climate Change. John Wiley & Sons, New York, NY,USA.

Sheel, V., Shyam Lal, a, Andreas Richter, b, Burrows, John P., 2010. Comparison of satellite observed tropospheric NO_2 over India with model simulations. Atmos. Environ. 44 (2010), 3314–3321.
Susskind, J., Barnet, C.D., Blaisdell, J.M., 2003. Retrieval of atmospheric and surface parameters from AIRS/AMSU/HSB data in the presence of clouds. IEEE Trans. Geosci. Rem. Sens. 41, 390–409.
Tanre, D., Kaufman, Y.J., Herman, M., Mattoo, S., 1997. Remote sensing of aerosol properties over oceans using the MODIS/EOS spectral radiances. J. Geophys. Res. 102, 16971–16986.
Tariq, S., Ali, M., 2015. Spatio-temporal distribution of absorbing aerosols over Pakistan retrieved from OMI onboard Aura satellite. Atmos. Pollut. Res. https://doi.org/10.5094/APR.2015.030.
Tariq, S., ul-Haq, Z., Ali, M., 2015. Analysis of optical and physical properties of aerosols during crop residue burning event of October 2010 over Lahore, Pakistan. Atmos. Pollut. Res. 6, 969–978. https://doi.org/10.1016/j.apr.2015.05.002.
Tariq, S., ul-Haq, Z., Ali, M., 2016. Satellite and ground-based remote sensing of aerosols during intense haze event of October 2013 over Lahore, Pakistan. Asia-Pacific J. Atmos. Sci. 52 (1), 25–33. https://doi.org/10.1007/s13143-015-0084-3.
ul-Haq, Z., Tariq, S., Ali, M., Mahmood, K., Batool, S.A., Rana, A.D., 2014. A study of tropospheric NO_2 variability over Pakistan using OMI data. Atmos. Pollut. Res. 5, 709–720. https://doi.org/10.5094/APR.2014.080.
ul-Haq, Z., Tariq, S., Ali, M., 2015. Tropospheric NO_2 trends over South Asia during the last decade (2004-2014) using OMI data. In: Advances in Meteorology (Special Issue: Satellite Observation of Atmospheric Compositions for Air Quality and Climate Study (SOAC), 959284, 18. https://doi.org/10.1155/2015/959284.
ul-Haq, Z., Tariq, S., Ali, M., 2016. Spatiotemporal patterns of correlation between atmospheric nitrogen dioxide and aerosols over South Asia. Meteorol. Atmos. Phys. https://doi.org/10.1007/s00703-016-0485-6.
ul-Haq, Z., Tariq, S., Ali, M., Rana, A.D., Mahmood, K., 2017. Satellite-sensed tropospheric NO_2 patterns and anomalies over Indus, Ganges, Brahmaputra, and Meghna river basins. Int. J. Rem. Sens. 38 (5), 1423–1450. https://doi.org/10.1080/01431161.2017.1283071.
UNEP, 2008. United Nations Environment Programme and Development Alternatives (2008), South Asia Environment Outlook 2009: UNEP, SAARC and DA. United Nations Environment Programme (UNEP).
US EPA, 2009. Assessment of the Impacts of Global Change on Regional U.S. Air Quality: a Synthesis of Climate Change Impacts on Ground-level Ozone. US EPA, Washington, DC.
Varotsos, C., Cartalis, C., Feidas, C., Gerasi, E., Asimakopoulos, D.N., 1992. Relationship of ozone and its precursors in the West Coast Air Basin of Athens: a statistical model for the assessment of air quality in an urban area. Atmos. Res. 28, 41–47.
Varotsos, C.A., Ondov, J.M., Efstathiou, M.N., Cracknell, A.P., 2014a. The local and regional atmospheric oxidants at Athens (Greece). Environ. Sci. Pollut. Res. 21, 4430. https://doi.org/10.1007/s11356-013-2387-1.
Varotsos, C., Christodoulakis, J., Tzanis, C., Cracknell, A.P., 2014b. Signature of tropospheric ozone and nitrogen dioxide from space: a case study for Athens, Greece. Atmos. Environ. 89, 721–730.
Veefkind, J.P., Boersma, K.F., Wang, J., Kurosu, T.P., Krotkov, N., Chance, K., Levelt, P.F., 2011. Global satellite analysis of the relation between aerosols and short-lived trace gases. Atmos. Chem. Phys. 11, 1255–1267.
Worden, H.M., Bowman, K.W., Kulawik, S.S., Aghedo, A.M., 2011. Sensitivity of outgoing longwave radiative flux to the global vertical distribution of ozone characterized by instantaneous radiative kernels from Aura-TES. J. Geophys. Res. 116, D14115 https://doi.org/10.1029/2010JD015101.